Author version: *J. Geophys. Res. (B: Solid Earth), vol.117; 2012; B04101, 19pp.*

Tectonics of the Ninetyeast Ridge derived from spreading records in adjacent oceanic basins and age constraints of the ridge

Kolluru S. Krishna[1], Honey Abraham[1], William W. Sager[2], Malcolm S. Pringle[3], Frederick Frey[3], Dasari Gopala Rao[4], Oleg V. Levchenko[5]

[1] National Institute of Oceanography, Council of Scientific and Industrial Research, Dona Paula, Goa – 403004, India
[2] Department of Oceanography, Texas A&M University, College Station, TX 77843-3146, USA
[3] Department of Earth and Planetary Sciences, Massachusetts Institute of Technology, Cambridge, MA 02139 USA
[4] Department of Geology, Osmania University, Hyderabad – 500007, India
[5] Shirshov Institute of Oceanology, Russian Academy of Sciences, Moscow 117997, Russian Federation

Abstract

Analysis of new and existing geophysical data for the Central Indian and Wharton Basins of the Indian Ocean was used to understand the formation and evolution of the Ninetyeast Ridge (NER), especially its relationship to the Kerguelen hot spot and the Wharton spreading ridge. Satellite gravity data and magnetic anomalies 34 through 19 define crustal isochrons and show fracture zones striking ~N 5˚E. One of these, at 89°E, crosses the ~N 10˚E trending-NER, impacting the NER morphology. From 77 to 43 Ma the NER lengthened at a rate of ~118 km/Myr, twice that of the ~48-58 km/Myr accretion rate of adjacent oceanic crust. This difference can be explained by southward jumps of the Wharton spreading ridge towards the hot spot, which transferred portions of crust from the Antarctic plate to the Indian plate, lengthening the NER. Magnetic anomalies document a small number of large spreading ridge jumps in the ocean crust immediately to the west of the NER, especially two leaving observable 65 and 42 Ma fossil spreading ridges. In contrast, complex magnetic anomaly progressions and morphology imply that smaller spreading ridge jumps occurred at more frequent

intervals beneath the NER. Comparison of the NER dates and magnetic anomaly ages implies that the hot spot first emplaced NER volcanoes on the Indian plate at a distance from the Wharton Ridge, but as the northward-drifting spreading ridge approached the hot spot, the two interacted, keeping later NER volcanism near the spreading ridge crest by spreading center jumps.

Key Words: Ninetyeast Ridge, Kerguelen hot spot, Ridge-hot spot interactions, Ridge Jumps, Ridge Migration

1. Introduction

The Ninetyeast Ridge (NER), one of the longest linear volcanic features on the Earth, extends ~5600 km in the N-S direction from 34°S to 17°N (Figure 1). Its southern part intersects the E-W trending Broken Ridge and the northern part (north of 10°N) is entirely buried under thick Bengal Fan sediments (Curray et al., 1982; Gopala Rao et al., 1997; Michael and Krishna, 2011), beneath which it converges upon the Andaman arc at about 17°N (Subrahmanyam et al., 2008). The ridge has an average width of 200 km and elevation of more than 2 km along most of its length (Sclater and Fisher, 1974; Fisher et al., 1982; Krishna et al., 1995, 2001a). The NER is often asymmetric in cross-section and ranges from low relief to high relief seamounts and linear ridge segments with some portions having a flat-topped morphology (Figure 2). Although numerous explanations have been proposed for the formation of the NER, it is widely accepted that the ridge was formed by Kerguelen hot spot volcanism when the hot spot was located beneath the Indian plate during the late Cretaceous and early Cenozoic (Peirce, 1978; Peirce, Weissel et al., 1989; Royer et al., 1991). This hypothesis is supported by new geochronology data generated for NER core samples from DSDP Leg 26 and ODP Leg 121 (Pringle et al., 2008), which show that the southern ridge is 43 Ma in age at DSDP Site 254 near the Broken Ridge and 77 Ma in age at ODP Site 758 near the north end of the NER and with a remarkably linear age progression in between (Figures 3a, b).

When compared to seafloor spreading in adjacent Central Indian and Wharton basins as delineated by seafloor spreading magnetic anomalies (e.g. Krishna et al., 1995, 1999), the new geochronology data (Pringle et al., 2008) reveal that the volcanic propagation rate (~118 km/ Myr) of the NER is double that of the half-spreading rates (48-58 km/ Myr) of the adjacent oceanic basins and, as a result, the NER is ~11° longer than the length of Indian plate created contemporaneously (Krishna et al., 1999). Previously Royer et al. (1991) and Krishna et al. (1995, 1999) have provided an explanation that the Wharton spreading ridge segments jumped southward several times, transferring lithosphere from Antarctic plate to the Indian plate. But the timing, location of the hot spot, and extent of these ridge jumps are uncertain because magnetic lineations near the NER are complex and magnetic data in the region are sparse.

In this study we compiled and modeled magnetic anomaly profile data from the NER and adjacent basins (Figures 3a and b) and examined the implications of newly available geochronology data from DSDP Leg 22 and ODP Leg 121 cores (Pringle et al., 2008). The geophysical data are mainly utilized for identification of magnetic patterns including fracture zones (FZs) and fossil ridge segments, of both the Wharton and Central Indian basins adjacent to the NER. With the derived tectonic constraints and geochronology data, we propose a model for interactions between the Wharton spreading center and the Kerguelen hot spot during the emplacement of the NER. Finally we discuss the mechanisms of NER accretion and why its length is much longer compared to that of the adjacent normal oceanic lithosphere formed during the same time interval.

2. NER Tectonic Setting

Major plate reorganizations of Indian Ocean seafloor spreading occurred at ~90 Ma and ~42 Ma, moving the Kerguelen hot spot alternately beneath the Indian and Antarctic plates, respectively (Liu et al., 1983). Initially, at approximately 120 Ma, the hot spot was beneath the Antarctic plate, leading to the formation of the southern and central parts of the Kerguelen Plateau and the Broken Ridge (Coffin et al., 2002). The first major plate reorganization, at ~90 Ma, placed the hot spot beneath the Indian plate and resulted in the accretion of the world's largest linear aseismic ridge, termed the NER. The second major plate reorganization, at ~42 Ma, relocated the hot spot beneath the Antarctic plate and resulted in the accretion of the Northern Kerguelen Plateau, including the Kerguelen Archipelago, and Heard and McDonald Islands (Coffin et al., 2002) since that time. It has been thought that during the formation of the NER, the Kerguelen hot spot was mostly located north of spreading ridge-segments that were part of the western extremity of the Wharton Ridge, which separated the Indian and Australian plates and was connected to the India-Antarctica Ridge through the 86°E transform fault (Krishna et al., 1995, 1999). Concurrently with the NER emplacement, the adjacent Wharton and Central Indian basins were also formed by the spreading of the Wharton and India-Antarctica ridges, respectively (Liu et al., 1983; Royer and Sandwell, 1989; Royer et al., 1991; Krishna et al., 1995, 1999). After the ~42 Ma plate reorganization, the Wharton spreading ridge effectively disappeared as the Southeast Indian Ridge formed, and the Indian and Australian plates merged together to form a single Indo-Australian plate (Liu et al., 1983; Krishna et al., 1995).

During Neogene time, a large diffuse plate boundary has formed in the central Indian Ocean, breaking the major Indo-Australian plate into three smaller component plates - Indian, Australian, and Capricorn plates (Royer and Gordon, 1997; Gordon et al., 1998). Almost the entire NER resides within this zone of complex deformation. Seismic results from Bengal Fan sediments reveal that the lithosphere within the boundary to the west of the NER displays reverse faulting (5–10-km-spaced faults) and long-wavelength (100–300 km) folding (Weissel et al., 1980; Bull, 1990; Chamot-Rooke et al., 1993; Krishna et al., 1998, 2001b). Using seismic stratigraphy and plate rotations, Krishna et al. (2009a) and Bull et al. (2010) subsequently determined that the lithospheric convergence began at 18-14 Ma within this plate boundary. Recent seismic results from the NER suggest that the ridge is dissected by numerous faults and experiencing ongoing deformation activity (Sager et al., 2010). Furthermore, the ridge is thought to be a structural partition that separates different styles of deformation in the Central Indian and Wharton basins (Deplus et al., 1998; Delescluse and Chamot-Rooke, 2007). Despite this ongoing tectonism, the overall deformation of the diffuse boundaries is small and thus can be ignored for our study of late Cretaceous and early Cenozoic plate boundary motions.

NER morphology is complex and varies along its length (Fisher et al., 1982; Krishna et al., 2001a; Sager et al., 2010). The southern ridge, south of 11°S, is tall, nearly continuous, and often highly asymmetric with a steep eastern slope and low western slope. In contrast, the ridge north of ~3°S consists of a series of mostly individual, large volcanoes with more symmetric cross-sections. In between, the ridge is low with a combination of small linear segments and seamounts (Krishna et al., 2001a). The position of the Kerguelen hot spot with respect to the Wharton spreading centers, the strike of oceanic fracture zones, plate motions, hot spot drift, variable hot spot magma output, and deformation-related faults are all factors that have been implicated as controls on the morphology of the NER (e.g., Royer et al., 1991).

3. Geophysical and Geological Data

An international scientific expedition was carried out onboard R/V *Roger Revelle* (KNOX06RR) during the year 2007 over the NER (Figure 2). During the cruise multibeam bathymetry, magnetic and gravity data, and 10-fold multichannel seismic reflection profiles, were acquired in the vicinity of ODP Site 758, DSDP Sites 216, 214 and 253 and at locations 6-8°S and 19°S. In addition to the geophysical data, basaltic rocks were also dredged at 22 sites along the NER (see Sager et al., 2007 for locations). Magnetic data utilized in this study were gathered from the KNOX06RR cruise, NGDC (National Geophysical Data Center) and NIO (National Institute of Oceanography) databases and the Trans Indian Ocean Geotraverse (TIOG) program (Table 1; Krishna et al., 1995). In addition we used newly determined $^{40}Ar/^{39}Ar$ radiometric ages (Pringle et al., 2008) of basaltic core samples from DSDP Sites 214, 216, 254 and ODP Sites 756-758 along the NER (Figures 3a, b).

4. Magnetic Anomaly Pattern of the Central Indian and Wharton Basins adjacent to the Ninetyeast Ridge

Magnetic anomaly profile data adjacent to the NER are plotted along ship-tracks and shown in Figures 3a and b. The data are overlaid on satellite free-air gravity data (Sandwell and Smith, 1997) in order to constrain precise positions of fracture zones (FZ), thereby constraining extrapolation of the magnetic lineations. The satellite gravity image clearly shows the presence of a number of nearly N-S trending narrow gravity features, indicating the signatures of FZ created during the northward movement of the Indian plate. From these gravity features, we have traced ten FZ between 80° and 97°E longitudes (Figures 3a and 3b). They trend in the N5°E direction, while the NER trends ~N10°E, consequently the 89°E FZ crosses the NER obliquely from east to west between 15°S and 10°S latitudes (Figures 3a and 3b). Magnetic anomalies are, in general, well developed with moderate amplitudes except over the NER and on its immediate east side (Figures 3a, 3b, 4a, 4b, and 4c). In particular between the 89°E FZ and 94°E FZ, the anomalies are modestly developed with lower amplitudes (Figures 3a, 3b, and 4b). The anomalies within this corridor seem to be subdued because of excessive seafloor undulations created by oceanic fracture zones, strike-slip displacements and vertical faulting (Pilipenko, 1996; Krishna et al., 2001a).

Earlier magnetic anomaly identifications from both the Central Indian and Wharton basins (Peirce, 1978; Liu et al., 1983; Pierce and Weissel et al., 1989; Royer et al., 1991; Krishna et al., 1995, 2009b; Krishna and Gopala Rao, 2000) were considered to determine the spreading rates and magnetic polarity chronology for the calculation of synthetic magnetic anomaly profiles. Half-spreading rates ranging from 2.3 to 8.5 cm/yr and geomagnetic polarity timescale (Cande and Kent, 1995) for the period from Late Cretaceous to early Tertiary were used to create synthetic magnetic anomaly models (shown in Figures 4a, 4b, and 4c). Following the anomaly pattern within the study area (west of the 86°E FZ, east of the 90°E FZ, and the region in between) three magnetic models were generated using the Matlab based MODMAG algorithm (Mendel et al., 2005) and correlated to the magnetic anomaly profiles for identification of seafloor spreading magnetic anomalies, thereby assigning ages to the oceanic crust. The magnetic anomaly sequences in model profiles, particularly anomalies 30 through 32n.2 and 21 through 24n.2, have characteristic shapes (see Figures 4a, 4b and 4c) generated by a unique arrangement of short-period geomagnetic polarity reversals. We used these distinctive anomaly shapes and patterns as reference picks for the correlation of observed anomalies to model profiles. With this approach most of our anomaly correlations have gained reasonably high confidence.

A comparison of the observed magnetic anomaly data of both the Central Indian and Wharton basins with synthetic model profiles (Figures 4a, 4b and 4c) leads to the identification of seafloor spreading anomalies 19 through 34, several fossil ridge segments, and a number of nearly N-S oriented FZ along 84°E, 85°E, 86°E, 89°E, 90°E, 92°E, 94°E, and 96°E longitudes. It is observed that half-spreading rates are significantly reduced, as low as 2.9 and 2.3 cm/yr, close to the end-phase of ridge segments at anomalies 30 and 19, respectively (Figures 4b and 4c). The ridge segments that ceased at anomaly 19 were part of the cessation of the entire Wharton spreading system, thereby contributing to the second major plate reorganization in the Indian Ocean and unification of Indian and Australian plates into a single major lithospheric plate. This event is thought to be a result of occurrence of continent-continent collision between India and Asia (Liu et al., 1983; Patriat and Segoufin, 1988). In regions to the west of the 86°E FZ and east of the NER, spreading anomalies 19 through 34 are identified with confidence and correlated with the anomaly picks from profile to profile (Figures 4a and 4b). To the west of the 86°E FZ magnetic lineations from 26 to 23n.1 are offset approximately along the 84°E and 85°E longitudes in a right-lateral sense by about 90 and 45 km, respectively, revealing the presence of oceanic fracture zones, termed as the 84°E FZ and 85°E FZ (Figures 5a and 5b). Likewise to the east of the NER the magnetic lineations from 32n.1 to 19 show large offsets approximately along 90°E, 92°E and 94°E longitudes in the opposite (left-lateral) sense by about 840, 820 and 150 km, respectively, revealing the presence of oceanic fracture zones, identified as the 90°E FZ, 92°E FZ and 94°E FZ (Figures 5a and 5b).

By comparison of the magnetic anomalies from profiles Wilkes815 (Pr. 9), sk82-02 (Pr. 3), dsdp22gc (Pr. 22), sk124-12 (Pr. 21), C1709 (Pr. 23), sk124-10 (Pr. 20), inmd06mv (Pr. 14), wilkes815 (Pr. 24), circ05AR-B (Pr. 46), tiog15 (Pr. 48), tiog16 (Pr. 49), circ05AR-C (Pr. 70), RC1402 (Pr. 32) and Wilkes907 (Pr. 71) with the synthetic magnetic model (Figure 4c), we identify symmetric pairs of anomaly sequences 30 through 32n.2 and 20 through 23n.1 on either side of anomaly signatures presumed to be associated with fossil ridge segments. These sequences evolved by the abandonment of ridge segments soon after anomaly 30 and at anomaly 19, respectively. In addition we identify anomalies 26 to 29 (increasing age towards the north) in between the aforesaid anomaly sequences, and anomalies 24n.2 and 25 on the south side of the younger anomaly sequence (Figures 4c, 5a, and 5b). Furthermore, minor dislocations, <50 km, are noted at two places, particularly in anomalies from 26 to 29 and 20 to 23n.2, and this led to recognition of smaller second-order fracture zones whose continuation is not observed in anomalies older than 30 (Figures 4c, 5a, and 5b). This suggests that these two fracture zones may have originated after magnetic anomaly 30 and continued up to anomaly 19. Thus the magnetic pattern in the corridor between the 86°E FZ and the NER has been disrupted by fracture zones and spreading ridge jumps, and as a result the magnetic pattern has become more complex in comparison to that of other regions west of the 86°E FZ and east of the NER. Previous studies have noted complex magnetic patterns west of the NER (Royer et al., 1991; Krishna et al., 1995; Krishna and Gopala Rao, 2000) and in the Wharton Basin (Liu et al., 1983) in broader perspective. In this study we generated more accurate magnetic anomaly maps for the basinal regions on both sides of much of the NER using up-to-date available magnetic anomaly profile data and satellite gravity anomaly data (Figures 5a and 5b), providing tighter constraints on the evolution of the NER and the interaction of the hot spot with spreading ridge segments.

Ages of the oceanic crust obtained from the magnetic lineations agree with ages of rock samples recovered at DSDP Site 215 in the Central Indian Basin and basal sediments sampled from DSDP Site 213 in the Wharton Basin, giving confidence in the anomaly identifications. The rock samples at DSDP Site 215 show 61 Ma age oceanic crust (Von der Borch et al., 1974a), which corresponds to magnetic anomaly 27 following the geomagnetic polarity timescale of Cande and Kent (1995). This is in good agreement with anomalies 26 and 28-29 in the vicinity of the Site 215 (Figure 5b). Likewise the oldest sediments at DSDP Site 213 are 57 Ma in age (Von der Borch et al., 1974b), which corresponds well with anomalies 25 and 26 on either side of the site.

The magnetic pattern in the vicinity of the NER reveals that the age of the oceanic crust to the west of the 86°E FZ increases towards the north from early Cenozoic to Late Cretaceous, while the crust to the east of the 92°E FZ increases its age in both north and south directions symmetric about the middle Eocene fossil Wharton Ridge segments. Contrasting to these trends, the crust in between these FZ shows a complex age succession with different age (65 and 42 Ma) fossil ridge segments (Figure 5). The ridge segments abandoned at anomaly 30 and at anomaly 19 by ridge jumps are identified in the equatorial region and in the area between 12° and 14°S latitudes, respectively.

5. Tectonic Evolution of the Ninetyeast Ridge

New $^{40}Ar/^{39}Ar$ ages of basaltic core samples from DSDP Sites 214, 216, 254 and ODP Sites 756-758 show that the NER is age progressive for a distance of 3980 km, north to south, spanning 77 to 43 Ma (Pringle et al., 2007, 2008). A plot of age versus latitude displays remarkable linearity (Figure 6), with age decreasing to the south and a volcanic propagation rate of 118 ± 5 km/Myr (Pringle et al., 2008). This contrasts with earlier dates that implied a significantly slower rate of 86 ± 12 km/Myr (Duncan, 1978, 1991). Comparison of the NER age progression with nearby magnetic anomalies indicates that the NER lengthened much more rapidly than adjacent lithosphere (Figure 6). In regions west of the 86°E FZ and east of the 90°E FZ, magnetic lineations 33 and 20, corresponding to approximately to 77 and 43 Ma, respectively, are separated by ~2000 km (Figure 6a), revealing that the crust was created at a rate of ~58 km/Myr. In other regions closer to NER (between 86°E FZ and NER; between 89°E FZ and 90°E FZ), the oceanic crust was formed at comparable rates ranging from 48 to 55 km/Myr (Figure 6b). This discrepancy is a result of the difference between relative plate velocity, recorded by seafloor magnetic lineations, and the volcanic propagation rate of the NER, which reflects the velocity of the Indian plate relative to the hot spot.

The propagation rate of NER volcanism is about twice that of the half-spreading rates recorded on the Indian plate, or similar to the full-spreading rate between the Antarctic and Indian plates. The motion of the Antarctic plate relative to the hot spot reference frame at this time was slow (Acton, 1999; Besse and Courtillot, 2002). Thus, relative to a nearly fixed Antarctic plate, the Indian plate was moving northward at about the full spreading rate, and the Wharton spreading center itself was migrating northward at about the half spreading rate. It would thus seem that the NER volcanic propagation simply records this full spreading rate as postulated previously (e.g., Royer et al., 1991). Because of its rapid northward drift relative to the NER hot spot, the Wharton spreading ridge should have simply crossed over the hot spot, and subsequent volcanism would have occurred on the Antarctic plate. However, the eruption ages for the NER core samples are similar to the nearby magnetic anomalies indicating that the Wharton spreading ridge remained relatively close to the hot spot throughout much of the NER history (Figure 6). This circumstance required that some tectonic mechanism acted to keep the spreading ridge close to the hot spot; we argue that ridge jumps are that mechanism.

5.1 Wharton Ridge Segments and Kerguelen Hot spot Interactions

Using an updated magnetic data set, we present an improved interpretation of magnetic anomalies, particularly immediately to the east and west of the NER (Figures 5a and 5b), which supersedes earlier anomaly identifications in this region (Sclater and Fisher, 1974; Liu et al., 1983; Royer et al., 1991; Krishna et al., 1995). From the trends of the FZ and the NER, it is found that the 89°E FZ crosses the NER obliquely between 15°S and 10°S latitudes (Figures 5a and 5b). Consequently the NER was formed in two different spreading corridors of oceanic crust: the north part of the ridge active before ~62 Ma is situated between the 89°E FZ and the 90°E FZ, while the south part of the NER is located between the 86°E FZ and the 89°E FZ.

As described in Section 4, the oceanic crust between the 86°E and 90°E FZs shows non-monotonic sequences of magnetic lineations caused by ridge jumps, with two major jumps occurring at 65 and 42 Ma (Figures 5a and 5b). At ~90 Ma, the Indian plate was bounded on the southwest side by the Wharton and India-Antarctica ridges, which were connected through the 86°E transform fault (Krishna et al., 1995) and the Kerguelen hot spot was located beneath the Indian plate at a moderate distance from the Wharton Ridge segments. During the first spreading reorganization during the Late Cretaceous, a ridge segment immediately west of the NER ceased its activity at ~65 Ma and jumped southward to a place between the locations of magnetic anomalies 33 and 32n.2. This spreading segment also broke into three smaller sub-segments. The ridge jump created a fossil ridge segment, now located near the equator (Figure 5a), and transferred oceanic crust from the Antarctic plate formed between magnetic anomalies just younger than 30 to just older than 32n.2 to the Indian plate (Figures 5a, 7b). During the second spreading jump at ~52 Ma, two sub-segments to the west of the NER jumped northward to crust formed between anomalies 25 and 26 (Figure 5b), and transferred oceanic crust from the Indian plate formed between magnetic anomalies just younger than 24n.2 to just older than 25 to the Antarctic plate (Figures 5b, 7d), while a third sub-segment closer to the NER appears to have jumped southward into pre-anomaly 34 oceanic crust. Finally, in the third spreading reorganization the entire Wharton Ridge system, including all three sub-segments, ceased spreading soon after middle Eocene anomaly 19. This process eventually led to unification of the Indian and Australian plates into a single Indo-Australian plate.

Considering the complex magnetic anomaly-derived age progression together with identified fossil ridge segments on both sides of the NER, the progression of ages determined from drill core samples (Figures 5 and 6), and proximity of the hot spot to spreading centers, we suggest two possible explanations for the ridge jumps with respect to the Kerguelen hot spot. With the observation of a few large ridge jumps to the west of the NER and the apparent continuity of the hot spot track, evolution of the NER may be explained by the positioning the Kerguelen hot spot beneath the Indian plate continuously from 77 to 43 Ma. This model requires a large amount of Antarctic plate lithosphere to be transferred to the Indian plate via spreading center jumps to the south away from the hot spot. Although this model appears to be simple because it allows the NER to form simply and with a monotonic age progression, the jumping of the ridge away from the hot spot appears counter to the widely-held idea that the excess heat and dynamic uplift over the hot spot weakens the lithosphere, causing the spreading center to jump toward the hot spot position. Observations on ridge-hot spot interactions at other locations led several researchers (Brozena and White, 1990; Small, 1995; Hardarson et al., 1997; Mittelstaedt et al., 2011) to conclude that ridge segments jump repeatedly towards a hot spot, even when the overall motion of the ridge may be away from the hotspot. It is thought that warm upper mantle temperatures weaken the lithosphere and the hot spot-imposed stress field provides necessary conditions for rifting. A possible explanation for the unusual behavior of the ridge jumps near the NER is that regional stress changes caused these ridge jumps, overriding local stresses caused by the hot spot.

An alternative model, which fits the notion of the spreading ridge jumping toward the hot spot, has the Wharton Ridge system drifting northward of the hot spot and the ridge segment beneath the NER repeatedly jumping back to the hot spot location, thereby accreting bits of the NER from the Antarctic plate to the Indian plate. NER components formed on the Antarctic plate should have reverse age progressions (i.e., become younger towards the north). The existing, reliable age data (Figure 6) are sparse, but remarkably consistent with a simple, linear age progression. Thus, if this explanation is true, reverse age segments must occur in the gaps between dated samples or the ridge jumps were frequent and small enough that the reversed age trends are not resolvable (Sager et al., 2010). Although it requires the added complexity of additional ridge jumps, we prefer this hypothesis because it allows the ridge segment to jump to the hot spot and it fits the observed hot spot-ridge offsets interpreted from magnetic lineations, which show the hot spot to the south of the Wharton Ridge during the Cenozoic (Figure 7).

Various stages of possible interactions between the spreading center and the Kerguelen hot spot during the formation of the NER are presented in Figure 8. Initially the hot spot was beneath the Indian plate and possibly at some distance from the spreading center, resulting in intraplate volcanism on the Indian plate now in the Bay of Bengal region (Figure 8a). This postulation is supported by the presence of regional lithospheric flexure determined beneath the NER in the Bay of Bengal region (Gopala Rao et al., 1997; Tiwari et al., 2003; Krishna et al., 2009b). Subsequently, rapid northward migration of the Wharton spreading ridge allowed it to coincide with the hot spot for on-axis volcanism (Figure 8b), which may have emplaced sections of NER simultaneously on both plates (with much of that formed on the Antarctic plate eventually captured via ridge jumps). Evidence of Kerguelen hot spot volcanism on the Antarctic plate during the formation of the NER is basalts from Skiff Bank (Kerguelen Plateau) dated at 68 Ma (Coffin et al., 2002).

Further spreading center migration would have placed the hot spot beneath the Antarctic plate for near ridge or ridge-flank volcanism (Figure 8c). With continued ridge migration, the hot spot moved farther from the spreading ridge beneath the Antarctic plate. The stress field created by the hot spot may have caused uplift and weakening of the overlying oceanic lithosphere, resulting in the initiation of rifting and spreading within the Antarctic plate and leading to southward ridge jumps. It is possible that hot spot material flowed along the base of the lithosphere to reach the spreading center for on-axis volcanism (Figure 8d), even when the hot spot was not located in the vicinity of the spreading ridge crest. This mechanism has been called upon to explain some features of the Amsterdam-St. Paul plateau, which is nearby and had a similar history of construction (Maia et al., 2011). In addition, the magnetic anomalies suggest that the NER formed within a relatively narrow spreading center corridor with long-offset FZ segments (Figure 7), and some NER volcanism may have occurred along the FZ or the long-offsets may have encouraged small bits to break off of the Antarctic plate (i.e., microplates or ridge jumps). The continuous process of hot spot-spreading ridge interaction may have provided necessary conditions to cause multiple ridge jumps. This behavior is also consistent with models of ridge-hot spot interaction in which ridge jumps are promoted by hot spot heating of the lithosphere and perturbations of the local stress field, and form preferentially in younger lithosphere in systems with relatively fast plate velocity (Mittelstaedt et al., 2008, 2011).

5.2 Evolution of Extra Length of the NER with respect to Simple Plate Drift

It is obvious from age data of the NER and adjacent oceanic crust evolved within the same time-frame (77 to 43 Ma) that the length of the NER is much greater than the stretch of the oceanic crust evolved on the Indian plate (Figure 6). The NER emplacement rate was almost a factor-of-two faster than the rate of accretion of oceanic crust. The extra length of the NER track is ~2000 km, and because the Wharton spreading ridge would have quickly passed the hot spot, it is necessary to postulate other explanations than simple plate drift. Furthermore, the linear trend of NER ages (Pringle et al., 2008) implies that significant slowing of the Indian plate, considered as a response of the continental collision between India and Asia, did not start until completion of construction of the entire NER (~42 Ma). Slow-spreading rates (2.4-2.9 cm/yr) observed in the present study (Figures 4b and 4c), particularly in two phases (anomalies 31 to 30 and again from 21 to 19) appear to indicate waning stages of ridge segments in the process of abandonment, but not a response to the slowing of the Indian plate motion.

As discussed in the previous section, the Kerguelen hot spot was initially in an off-ridge position during the formation of the NER in the Bay of Bengal region (Figure 8a), therefore the Wharton spreading ridge may have taken considerable time to reach the position of the hot spot and to move away to the north. In the process, the northern part of the NER, at least down to 5°N latitude, was created by two different plate motions, viz., by plate motion relative to the hot spot and by a plate boundary (Wharton spreading ridge) migration. The latter activity may have added some additional length of volcanic constructs to the NER track. During the emplacement of the central part of the NER, particularly from 5°N to 11°S latitudes, the hot spot and ridge segments were often in close proximity and this may have allowed the hot spot to form components of the NER on the Antarctic plate that were subsequently transferred to the Indian plate through southward ridge jumps (Figure 7b-d).

A critical question for NER evolution is how many such ridge jumps occurred. Our interpretation of the magnetic data set in basins adjacent to the NER is a small number of larger ridge jumps. However, both Krishna et al. (1999) and Desa et al. (2009) have mapped smaller southward ridge jumps near the NER at ~76 and 54 Ma, respectively. Sager et al. (2010) concluded, based on identification of extensive faulting within the NER structure, that numerous small-scale ridge jumps may have occurred and that the hot spot and Wharton spreading ridge may have remained in close proximity. Small ridge jumps are an attractive solution to the paradox that large ridge jumps would result in long segments of reversed age trend yet existing age data are remarkably linear (Figure 6). Such ridge jumps may also explain the apparent increased FZ offsets during the Cenozoic on the Wharton Ridge near NER (Figure 7).

Although it is true that existing NER age data are sparse and might not detect a reversed age segment, the deviant segment would have to hiding in the gaps of the current data. Further, magnetic anomalies near the NER are very difficult to interpret (Figure 3) presumably because the extended history of hot spot and spreading center volcanism does not result in simple magnetization of the ocean crust and discernable patterns of magnetic anomalies. Another factor is that small ridge jumps can be difficult to detect because this requires the recognition of a repeated anomaly pattern that may not be clear unless there are several mirrored anomalies (i.e., a seafloor spreading for a significant time). Thus, despite the improvement with the current magnetic dataset over prior compilations, it is not surprising that small ridge jumps are not recognized in the pattern of magnetic anomalies along the NER. More detailed magnetic surveys with closely spaced data would be needed to recognize of small jumps, as shown, for example, at Amsterdam-St. Paul Plateau (Maia et al., 2011).

Besides the processes discussed above, absolute hot spot movement also may have contributed to the lengthening of the NER. Paleomagnetic analyses and mantle flow models have been used to infer 7-10° (800-1100 km) of southward motion of the Kerguelen hot spot during the past 120 Myr (Klootwijk et al., 1991; Antretter et al., 2002; O'Neill et al., 2003). Such southward motion would also lengthen the NER, but we cannot quantify the north-south hot spot motion because our data set only shows the relative motions of the hot spot and spreading center.

6. Summary and conclusions

An investigation of magnetic anomaly profiles and other geophysical data around the NER and adjacent Central Indian and Wharton basins together with newly determined radiometric ages from igneous rocks cored at DSDP and ODP Sites on the NER has provided new insights on the evolution of the NER and interactions between the Wharton spreading ridge segments and the Kerguelen hot spot. Important observations are as follows.

1. Magnetic anomaly studies of both the Central Indian and Wharton basins have provided locations of magnetic lineations from 19 through 34 and fossil ridge segments which ceased spreading at 65 and 42 Ma. The lineation offsets are further constrained by narrow, linear gravity anomalies within satellite-derived gravity data that we interpret as fracture zone features. The NER trends ~N 10°E and obliquely crosses ~N 5°E oriented fracture zones. Thus in the south, the 89°E FZ borders the NER on the east side, whereas in the north the same fracture zone borders the ridge on the west side. In the central part between 11°S and 18°S, the fracture zone obliquely crosses the NER.
2. The age of oceanic crust to the west of the 86°E FZ (Central Indian Basin) increases towards the north from early Cenozoic to Late Cretaceous, while the crust to the east of the 90°E FZ (Wharton Basin) increases its age in both the north and south directions about 42 Ma fossil Wharton Ridge segments. Contrasting to these

patterns, the crust between the FZs near the NER shows a complex age succession together with fossil ridge segments of different ages (65 and 42 Ma).

3. Comparison of ages of oceanic crust, directly to the east and west of the NER with newly determined radiometric ages at DSDP Sites 216, 214, 254 and ODP Sites 756-758 shows that the NER lengthened at a rate twice that of adjacent oceanic crust.

4. The resulting difference in lengths of the NER (~3980 km) and adjacent oceanic crust (~2000 km) constructed from 77 to 43 Ma is remarkable and requires a geodynamical explanation. During the formation of the NER, the distance between the Kerguelen hot spot and spreading ridge segments changed due to the northward migration of the Wharton spreading ridge, southward ridge jumps, and possibly southward motion of the hot spot. Spreading ridge migration probably resulted in the Kerguelen hot spot underlying the Antarctic plate during the early Cenozoic, and led to formation of volcanic edifices on the Antarctic plate by ridge-flank volcanism and by lateral transport of hot spot melt along the ridge-axis. The southward ridge jumps transferred parts of the NER originally formed on the Antarctic plate to the Indian plate and were the major the major contribution to the extra lengthening of the NER.

Acknowledgments

We are indebted to captain, ship crew, and technicians of the R/V *Roger Revelle* for their efforts during the international scientific expedition (KNOX06RR) of the Ninetyeast Ridge. The field program was supported by the National Science

Foundation Grants OCE-0550743 and OCE-05499852. Honey Abraham is thankful to CSIR, New Delhi, for the support of student research fellowship (NET-JRF). DGR is thankful to DST, New Delhi for supporting his research activities through DST-RFBR project 1103. We thank Jon Bull, Chuck DeMets and anonymous Associate Editor for their critical comments and suggestions on the manuscript, with which the manuscript has improved greatly. This is NIO contribution number xxxx.

References:

Acton, G. D., (1999), Apparent polar wander of India since the Cretaceous with implications for regional tectonics and true polar wander, *Mem. Geol. Soc. India*, 44, 129-175.

Antretter, M., B. Steinberger, F. Heider, and H. Soffel (2002), Paleolatitudes of the Kerguelen hot spot: new plaeomagnetic results and dynamic modeling, *Earth Planet. Sci. Lett.*, 203, 635-650.

Besse, J., and V. Courtillot (2002), Apparent and true polar wander and the geometry of the geomagnetic field over the last 200 Myr, *J. Geophys. Res.*, 107(B11), 2300, doi:10.1029/2000JB000050,.

Brozena, J. M., and R. White (1990), Ridge jumps and propagations in the South Atlantic Ocean, *Nature*, 348, 149–152, doi:10.1038/348149a0.

Bull, J. M. (1990), Structural style of intraplate deformation, Central Indian Ocean Basin: evidence for the role of fracture zones, *Tectonophysics*, 184, 213-228.

Bull J. M., C. DeMets, K. S. Krishna, D. J. Sanderson, and S. Merkouriev (2010), Reconciling plate kinematic and seismic estimates of lithospheric convergence in the central Indian Ocean, *Geology*, 38, 307-310.

Cande, S. C., and D. V. Kent (1995), Revised calibration of the geomagnetic polarity time scale for the late Cretaceous and Cenozoic, *J. Geophys. Res.*, 100, 6093-6095.

Chamot-Rooke, N., F. Jestin, B. de Voogd, and Phedre Working Group (1993), Intraplate shortening in the central Indian Ocean determined from a 2100-km-long north-south deep seismic reflection profile, *Geology*, 21, 1043-1046.

Coffin, M. F., M. S. Pringle, R. A. Duncan, T. P. Gladczenko, M. Storey, R. D. Müller, and L. A. Gahagan (2002), Kerguelen hot spot magma output since 130 Ma, *J. Petrology*, 43, 1121-1139.

Curray, J. R., F. J. Emmel, D. G. Moore, and W. R. Russel (1982), Structure, tectonics, and geological history of the northeastern Indian Ocean, in The Ocean Basins and Margins, vol. 6, *The Indian Ocean*, A. E. Nairn and F. G. Stheli (eds.), pp. 399–450, Plenum, New York.

Delescluse, M., and N. Chamot-Rooke (2007), Instantaneous deformation and kinematics of the India-Australia plate, *Geophys. J. Int.*, 168, 818–842.

Deplus, C., M. Diament, H. Hebert, G. Bertrand, S. Dominguez, J. Dubois, J. Malod, P. Patriat, B. Pontoise, and J.J. Sibilla (1998), Direct evidence of active deformation in the eastern Indian oceanic plate, *Geology*, 26, 131-134.

Desa, M., M. V. Ramana, and T. Ramprasad (2009), Evolution of the Late Cretaceous crust in the equatorial region of the Northern Indian Ocean and its implication in understanding the plate kinematics, *Geophys. J. Int.*, 177, 1265–1278.

Duncan, R. A. (1978), Geochronology of basalts from the Ninetyeast Ridge and continental dispersion in the eastern Indian Ocean, *J. Volc. Geotherm. Res.*, 4, 283-305.

Duncan, R.A. (1991), Age distribution of volcanism along aseismic ridges in the eastern Indian Ocean, *Proc. ODP, Sci. Res.*, 121 507-517.

Fisher R. L., M. J. Jantsch, and R. L. Comer (1982), General Bathymetric chart of the Oceans (GEBCO); Canadian Hydrographic Service, Ottawa, Canada.

Gopala Rao, D., K. S. Krishna, and D. Sar (1997), Crustal evolution and sedimentation history of the Bay of Bengal since the Cretaceous, *J. Geophys. Res.*, 102, 17,747–17,768, doi:10.1029/96JB01339.

Gordon, R. G., C. DeMetes, and J.-Y. Royer (1998), Evidence for long-term diffuse deformation of the lithosphere of the equatorial Indian Ocean, *Nature*, 395, 370-374.

Hardarson, B. S., J. G. Fitton, R. M. Ellam, and M. S. Pringle (1997), Rift relocation - a geochemical and geochronological investigation of a paleorift in northwest Iceland, *Earth Planet. Sci. Lett.,* 153, 181–196, doi:10.1016/S0012-821X(97)00145-3.

Klootwijk, C. T., S. G. Jeff, J. W. Peirce, and G. M. Smith (1991), Constraints on the Indian-Asia convergence: Paleomagnetic results from Ninetyeast Ridge, in: J. K. Weissel, J. W. Pierce, E. Taylor and J. Alt (Eds.), *Proc. ODP, Sci. Results*, 121, 777-882.

Krishna, K. S., D. Gopala Rao, M. V. Ramana, V. Subrahmanyam, K. V. L. N. S. Sarma, A. I. Pilipenko, V. S. Shcherbakov, and I. V. Radhakrishna Murthy (1995), Tectonic model for the evolution of oceanic crust in the northeastern Indian Ocean from the Late Cretaceous to the early Tertiary, *J. Geophys. Res.*, 100, 20,011–20,024, doi:10.1029/94JB02464.

Krishna, K. S., M. V. Ramana, D. Gopala Rao, K. S. R. Murthy, M. M. Malleswara Rao, V. Subrahmanyam, and K. V. L. N. S. Sarma (1998), Periodic deformation of oceanic crust in the central Indian Ocean, *J. Geophys. Res.*, 103, 17,859–17,875, doi:10.1029/98JB00078.

Krishna, K. S., D. Gopala Rao, L. V. Subba Raju, A. K. Chaubey, V. S. Shcherbakov, A. I. Pilipenko, and I. V. Radhakrishna Murthy (1999), Paleocene on-axis hot spot volcanism along the Ninetyeast Ridge: An interaction between the Kerguelen hot spot and the Wharton spreading center, *Proc. Indian Acad. Sci. (Earth Planet. Sci.),* 108, 255–267.

Krishna, K. S., and D. Gopala Rao (2000), Abandoned Paleocene spreading center in the northeastern Indian Ocean: Evidence from magnetic and seismic reflection data, *Mar. Geol.*, 162, 215–224, doi:10.1016/S0025-3227(99)00085-7.

Krishna, K.S., Y.P. Neprochnov, D. Gopala Rao, and B. N. Grinko (2001a), Crustal structure and tectonics of the Ninetyeast Ridge from seismic and gravity studies, *Tectonics*, 20, 416 – 433, doi:10.1029/2001TC900004.

Krishna, K. S., J. M. Bull, and R. A. Scrutton (2001b), Evidence for multiphase folding of the central Indian Ocean lithosphere, *Geology*, 29, 715–718, doi:10.1130/0091-7613(2001).

Krishna, K. S., J. M. Bull, and R. A. Scrutton (2009a), Early (pre-8 Ma) fault activity and temporal strain distribution in the central Indian Ocean, *Geology*, 37, 227–230.

Krishna K. S., L. Michael, R. Bhattacharyya, and T. J. Majumdar (2009b), Geoid and gravity anomaly data of conjugate regions of Bay of Bengal and Enderby Basin - new constraints on breakup and early spreading history between India and Antarctica, *J. Geophys. Res.*, 114, B03102, doi:10.1029/2008JB005808.

Liu, C. S., J. R. Curray, and J. M. McDonald (1983), New constraints on the tectonic evolution of the Eastern Indian Ocean, *Earth Planet. Sci. Lett.*, 65, 331-342.

Maia, M., I. Pessanha, E. Courreges, M. Patriat, P. Gente, C. Hémond, M. Janin, K. Johnson, W. Roest, J-Y. Royer, and J. Vetteville (2011), Building of the Amtersdam-St. Paul plateau: A 10 Myr history of a ridge-hot spot interaction and variations in the strength of the hot spot source, *J. Geophys. Res.,* 116, B09104, doi:10.1029/2010JB007768.

Mendel, V., M. Munschy, and D. Sauter (2005), MODMAG, a MATLAB program to model marine magnetic anomalies, *Comput. & Geosci.,* 589–597.

Michael, L., and K. S. Krishna (2011), Dating of the 85°E Ridge (northeastern Indian Ocean) using marine magnetic anomalies, *Curr. Sci.*, 100, 1314-1322.

Mittelstaedt, E., G. Ito, and M. D. Behn (2008), Mid-ocean ridge jumps associated with hot spot magmatism, *Earth Planet. Sci. Lett.*, 266, 256-270.

Mittelstaedt, E., G. Ito, and J. van Humen (2011), Repeat ridge jumps associated with plume-ridge interaction, and ridge migration, *J. Geophys. Res.*, 116, B01102, doi:10.1029/2010JB007504.

O'Neill, C., D. Müller, and B. Steinberger (2003), Geodynamic implications of moving Indian Ocean hot spots, *Earth Planet. Sci. Lett.*, 215, 151-168.

Patriat, P., and J. Segoufin (1988), Reconstruction of the central Indian Ocean, *Tectonophysics*, 155, 211-234.

Peirce, J. W. (1978), The northward motion of India since the late Cretaceous, *Geophys. J. Royal Astro. Soc. J.*, 52, 277-311.

Peirce, J. W., J. K. Weissel et al., (1989), *Proc. ODP, Init. Repts.*, 121, pp.1000.

Pilipenko, A. I. (1996), Fracture zones of the Ninetyeast Ridge area, Indian Ocean, *Geotectonics*, 30, 441-451.

Pringle, M. S., F. A. Frey, E. M. Mervine, and W. W. Sager (2007), New Ar/Ar ages from the Ninetyeast Ridge, Indian Ocean: Beginning of a robust Indo-Atlantic hot spot reference frame, *EOS, Trans. AGU, 88* (52), Fall Mtg. Supplement, abstract U13A-0871.

Pringle, M. S., F. A. Frey, and E. M. Mervine (2008), A simple linear age progression for the Ninetyeast Ridge, Indian Ocean: New constraints on Indian plate motion and hot spot dynamics, *EOS, Trans. AGU, 89* (53) Fall Mtg. Suppl., abstract T54B-03.

Royer, J.-Y., and D. T. Sandwell (1989), Evolution of the eastern Indian Ocean since the late Cretaceous: Constraints from Geosat altimetry, *J. Geophys. Res.*, 94, 13,755–13,782, doi:10.1029/JB094iB10p13755.

Royer, J.-Y., J. W. Peirce, and J. K. Weissel (1991), Tectonic constraints on the hot-spot formation of Ninetyeast Ridge, *Proc. ODP, Sci. Res.*, 121, 763-776.

Royer, J.-Y., and R.G. Gordon (1997), The motion and boundary between the Capricorn and Australian plates, *Science*, 277, 1268 – 1274, doi:10.1126/science.277.5330.1268.

Sandwell, D. T., and W. H. F. Smith (1997), Marine gravity from Geosat and ERS-1 satellite altimetry, *J. Geophys. Res.*, 102, 10039-10054.

Sclater, J. G., and R. L. Fisher (1974), Evolution of the east central Indian Ocean, with emphasis on the tectonic setting of the Ninetyeast Ridge, *Geol. Soc. Am. Bull.*, 85, 683-702.

Sager, W.W. et al., (2007), Cruise Report KNOX06RR R/V Roger Revelle, pp. 1-82. (http://earthref.org/erda/1172).

Sager, W. W., C. F. Paul, K. S. Krishna, M. Pringle, A. E. Eisin, F. A. Frey, D. Gopala Rao, and O. Levchenko (2010), Large fault fabric of the Ninetyeast Ridge implies near-spreading ridge formation, *Geophys. Res. Lett.*, 37, L17304, doi:10.1029/ 2010GL044347.

Small, C. (1995), Observation of ridge–hot spot interactions in the Southern Ocean, *J. Geophys. Res.*, 100, 17931–17946.

Subrahmanyam, C., R. Gireesh, S. Chand, K. A. Kamesh Raju, and D. Gopala Rao (2008), Geophysical characteristics of the Ninetyeast Ridge – Andaman island arc/ trench convergent zone, *Earth Planet. Sci. Lett.*, 266, 29-45.

Tiwari, V. M., M. Diament, and S. C. Singh (2003), Analysis of satellite gravity and bathymetry data over Ninety-East Ridge: variation in the compensation mechanism and implication for emplacement process, *J. Geophys. Res.*, 108(B2), 2109, doi:10.1029/ 2000JB000047.

Von der Borch, C. C., J. G. Sclater et al., (1974a), Site 215*, Init. Repts. DSDP,* 22, 193-211.

Von der Borch, C. C., J. G. Sclater et al., (1974b), Site 213, *Init. Repts. DSDP*, 22, 193-211.

Weissel, J. K., R. N. Anderson, and C. A. Geller (1980), Deformation of the Indo-Australian plate, *Nature*, 287, 284-291.

Figure Captions:

Figure 1: General bathymetry of the Indian Ocean showing mid-oceanic ridge systems, oceanic basins, aseismic ridges and plateaus. Numbered solid triangles and circles show DSDP and ODP sites, respectively, that are mentioned in the text. BR = Broken Ridge, CR = Carlsberg Ridge, CIR = Central Indian Ridge, SWIR = Southwest Indian Ridge, SEIR = Southeast Indian Ridge.

Figure 2: Magnetic tracks in the vicinity of the NER. Red solid-lines indicate magnetic profiles acquired from different data sources (KNOX06RR cruise, NGDC, NIO and TIOG databases; the key of profile identifiers with specific cruises is given in Table 1), which are analyzed in the present study. Detailed geophysical data including multibeam bathymetry, 10-fold multichannel seismic reflection, and magnetic profiles were acquired in locations represented by yellow-colored rectangles on top of the NER. Solid triangles and circles indicate DSDP and ODP drill sites, respectively.

Figure 3: Magnetic anomaly profiles shown on top of the satellite free-air gravity image of the northeastern Indian Ocean (prepared from database of Sandwell and Smith, 1997). The map is divided into two parts for better visualization.

(a) Magnetic anomaly data are plotted along the ship tracks. White dashed lines are drawn to follow narrow gravity features that define oceanic fracture zones. DSDP and ODP sites are shown by solid red triangles and solid black circles, respectively. Ages indicated at each drill site are from the geochronology data published by Pringle et al. (2008).

(b) Southern part of the satellite gravity and magnetic anomaly profile data of the northeastern Indian Ocean.

Figure 4: Observed magnetic anomaly profile data are correlated with synthetic magnetic profiles.

(a) West of the 86°E FZ. Spreading-type magnetic anomalies 21 through 34 are identified and correlated from profile to profile. The geomagnetic polarity time scale of Cande and Kent (1995) was used for assigning the age to the magnetic lineations.

(b) East of the NER. Magnetic anomalies 20 through 34 and fossil ridge segments (of middle Eocene age) are identified. The offsets in magnetic lineations are used to define several fracture zones. Hashed lines (“FRS”) denote abandoned (“fossil”) spreading centers

(c) Between the 86°E FZ and the NER. Magnetic anomalies 21 through 34 are identified and fossil ridge segments (FRS) of latest Cretaceous and middle Eocene age are identified. The magnetic lineations identified between the FRS have lost systematic continuity in anomaly sequence due to ridge jumps.

Figure 5: Interpreted magnetic lineations (black lines), fossil ridge segments (solid stippled line) and oceanic fracture zones (dashed lines) of the northeastern Indian Ocean. Magnetic lineations indicated with blue lines are adopted from earlier studies (Royer et al., 1991; Krishna and Gopala Rao, 2000). The tectonic map is divided into two parts for better visualization. Magnetic profiles are shown particularly to support the anomaly identifications, correlations and offsets. Fracture zones are tightly constrained by satellite

gravity data. Bathymetric contour 3000 m and less water depths are shaded for outlining the physiography of the NER and other features. (a) northern NER; (b) southern NER.

Figure 6: Comparison of rates of ocean crust creation in different spreading corridors and the volcanic propagation rate on the NER. (a) Seafloor created in the Central Indian and Wharton basins, west of the 86ºE and east of the 92ºE fracture zones, respectively. (b) Radiometric ages from DSDP and ODP sites along the NER, seafloor created immediately to the west between the 88ºE and 89ºE fractures zones, and seafloor created immediately to the east between the 89ºE and 90ºE fracture zones. Black solid-dots show ages of drill core samples (Pringle et al, 2008); open symbols denote seafloor spreading magnetic anomalies (Figure 4 & 5). FRS indicates fossil ridge segment. Note the northward spreading center jump in the seafloor between the 86ºE and 88ºE fracture zones after C24n.2 time into C25 age crust, and subsequent spreading up to the FRS just after C20.

Figure 7: Tectonic evolution of the NER with respect to adjacent spreading ridge segments for four different ages from the late Cretaceous to early Cenozoic. Solid line shows the relatively well-constrained location of the Wharton spreading centers and transform faults on either side of the NER. Dashed line represents the Wharton spreading segment active directly under the NER at that time; its location is only approximate because the complex volcanic history of the crust directly under the NER did not allow the formation of discernable magnetic anomaly patterns. Two episodes of spreading center jumps and transferred crust can be specifically identified directly to the west

of the NER. The more frequent, smaller spreading center jumps proposed for the corridor directly under the NER cannot be specifically identified, but those corridors should include about 50% crust transferred from the Antarctic (ANT) to Indian (IND) plates.

Figure 8: Sketch model showing possible interactions between the Kerguelen hot spot, proximal ridge segments and oceanic lithosphere during the formation of the NER. The model is developed based on the conceptual model of Mittelstaedt et al. (2011) and the results obtained from the present study. (a) Off-axis volcanism when the hot spot was located north of the spreading ridge segments; (b) On-axis volcanism when the hot spot was located at the spreading ridge after northward migration of the plate boundary (Wharton Ridge) with respect to a nearly fixed Antarctic plate; (c) Volcanism on the ridge flank when the hot spot was located beneath the weak lithosphere of the Antarctic plate; and (d) On-axis melt flow when the hot spot was located off-axis beneath older-age lithosphere of the Antarctic plate.

Table 1: Details of profiles ids and data bases used in the present study

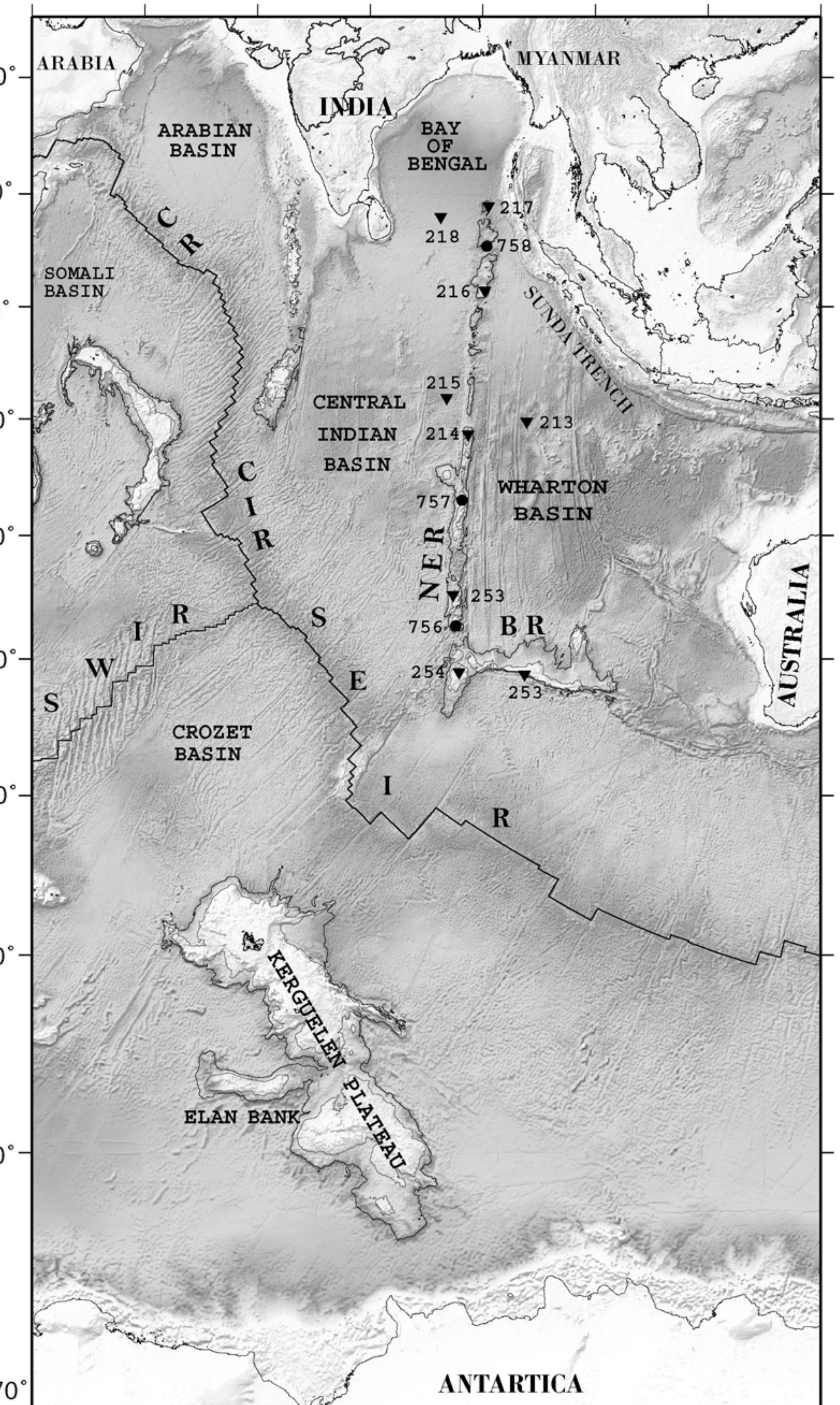
ARABIA
MYANMAR
INDIA
ARABIAN BASIN
BAY OF BENGAL
SOMALI BASIN
217
218
758
216
SUNDA TRENCH
215
CENTRAL INDIAN BASIN
213
214
757
WHARTON BASIN
NER
253
756
B R
254
253
AUSTRALIA
CR
CIR
SWIR
SEIR
CROZET BASIN
KERGUELEN PLATEAU
ELAN BANK
ANTARTICA
20° N
10°
0°
10°
20°
30°
40°
50°
60°
70° S
50°E
60°
70°
80°
90°
100°
110°
120°

Figure 1

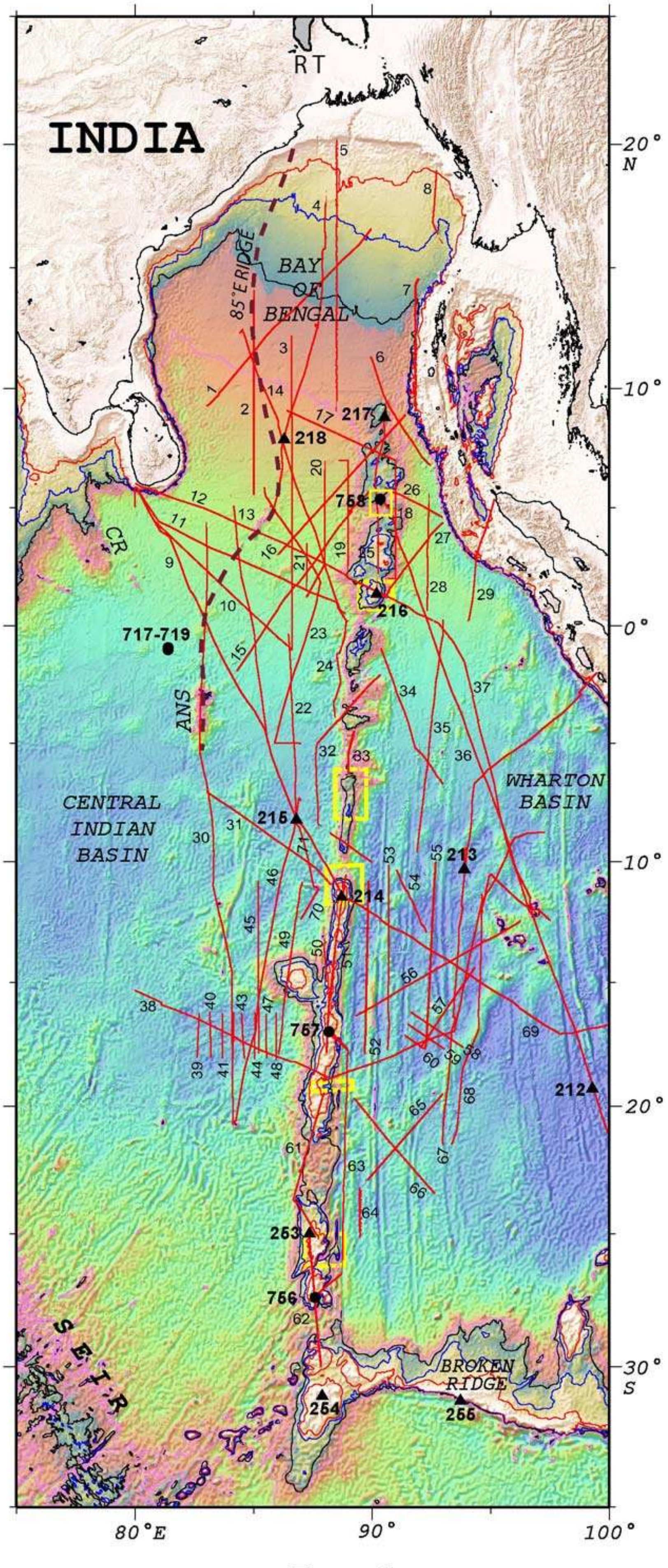
INDIA
RT
BAY OF BENGAL
85°E RIDGE
CR
ANS
CENTRAL INDIAN BASIN
WHARTON BASIN
BROKEN RIDGE
SEIR
717-719
217
218
758
216
215
214
213
212
757
253
756
254
255
20° N
10°
0°
10°
20°
30° S
80°E
90°
100°

Figure 2

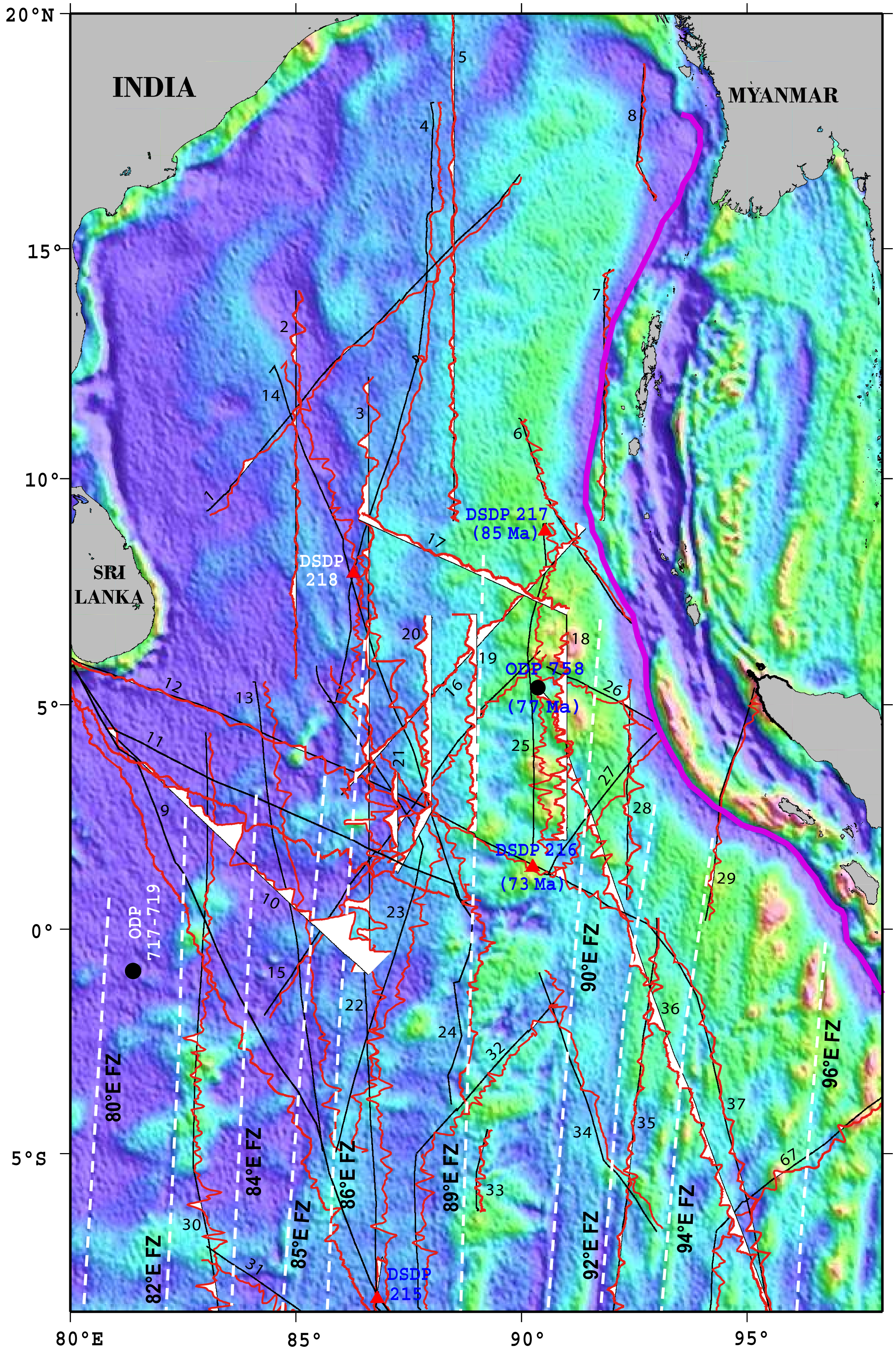

INDIA
MYANMAR
SRI LANKA
20°N
15°
10°
5°
0°
5°S
80°E
85°
90°
95°
DSDP 217
(85 Ma)
DSDP 218
ODP 758
(77 Ma)
DSDP 216
(73 Ma)
ODP 717-719
DSDP 215
80°E FZ
82°E FZ
84°E FZ
85°E FZ
86°E FZ
89°E FZ
90°E FZ
92°E FZ
94°E FZ
96°E FZ
1
2
3
4
5
6
7
8
9
10
11
12
13
14
15
16
17
18
19
20
21
22
23
24
25
26
27
28
29
30
31
32
33
34
35
36
37
67

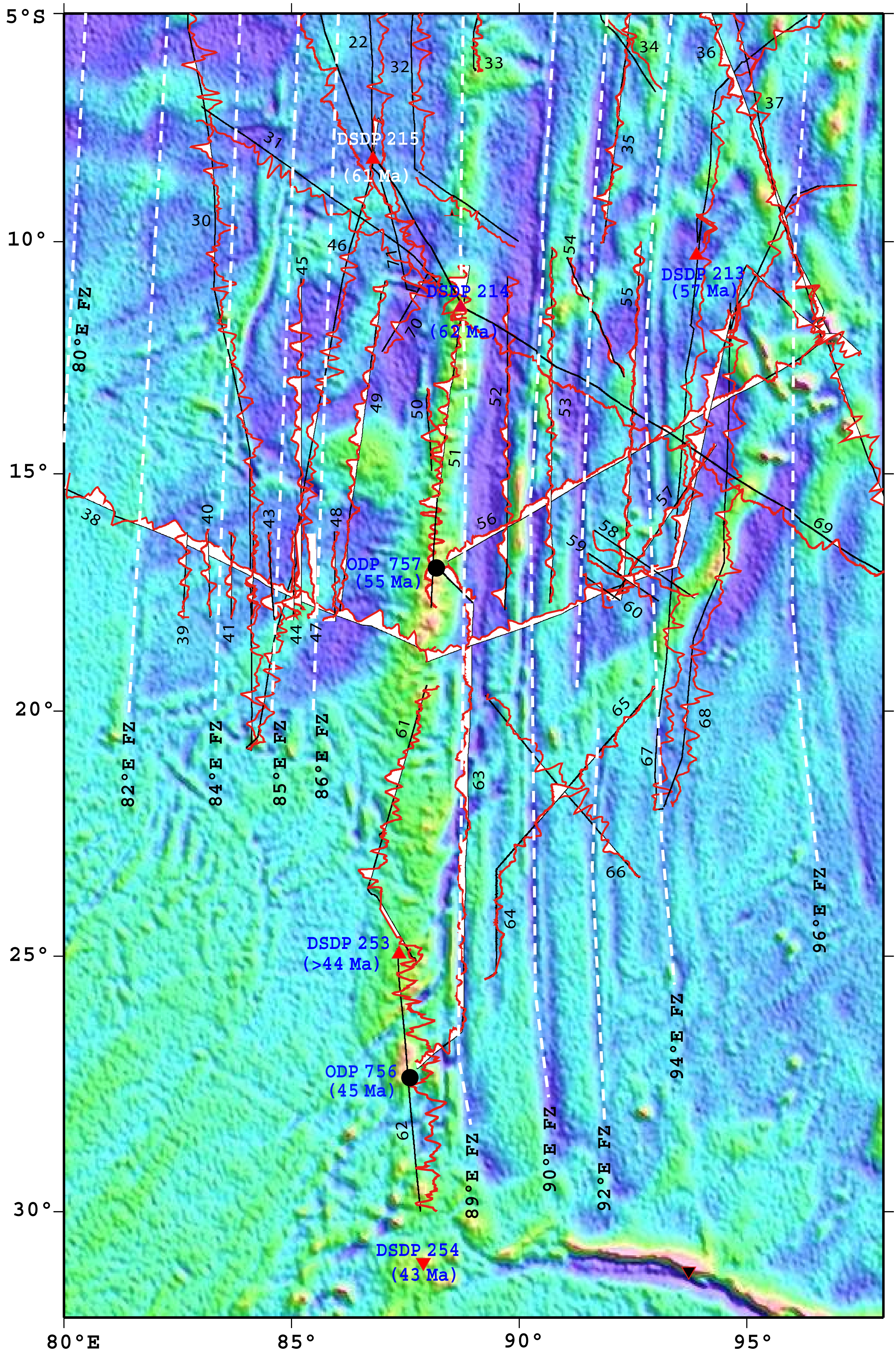
5°S
10°
15°
20°
25°
30°
80°E
85°
90°
95°
DSDP 215
(61 Ma)
DSDP 214
(62 Ma)
DSDP 213
(57 Ma)
ODP 757
(55 Ma)
DSDP 253
(>44 Ma)
ODP 756
(45 Ma)
DSDP 254
(43 Ma)
80°E FZ
82°E FZ
84°E FZ
85°E FZ
86°E FZ
89°E FZ
90°E FZ
92°E FZ
94°E FZ
96°E FZ
22
30
31
32
33
34
35
36
37
38
39
40
41
43
44
45
46
47
48
49
50
51
52
53
54
55
56
57
58
59
60
61
62
63
64
65
66
67
68
69
70
71

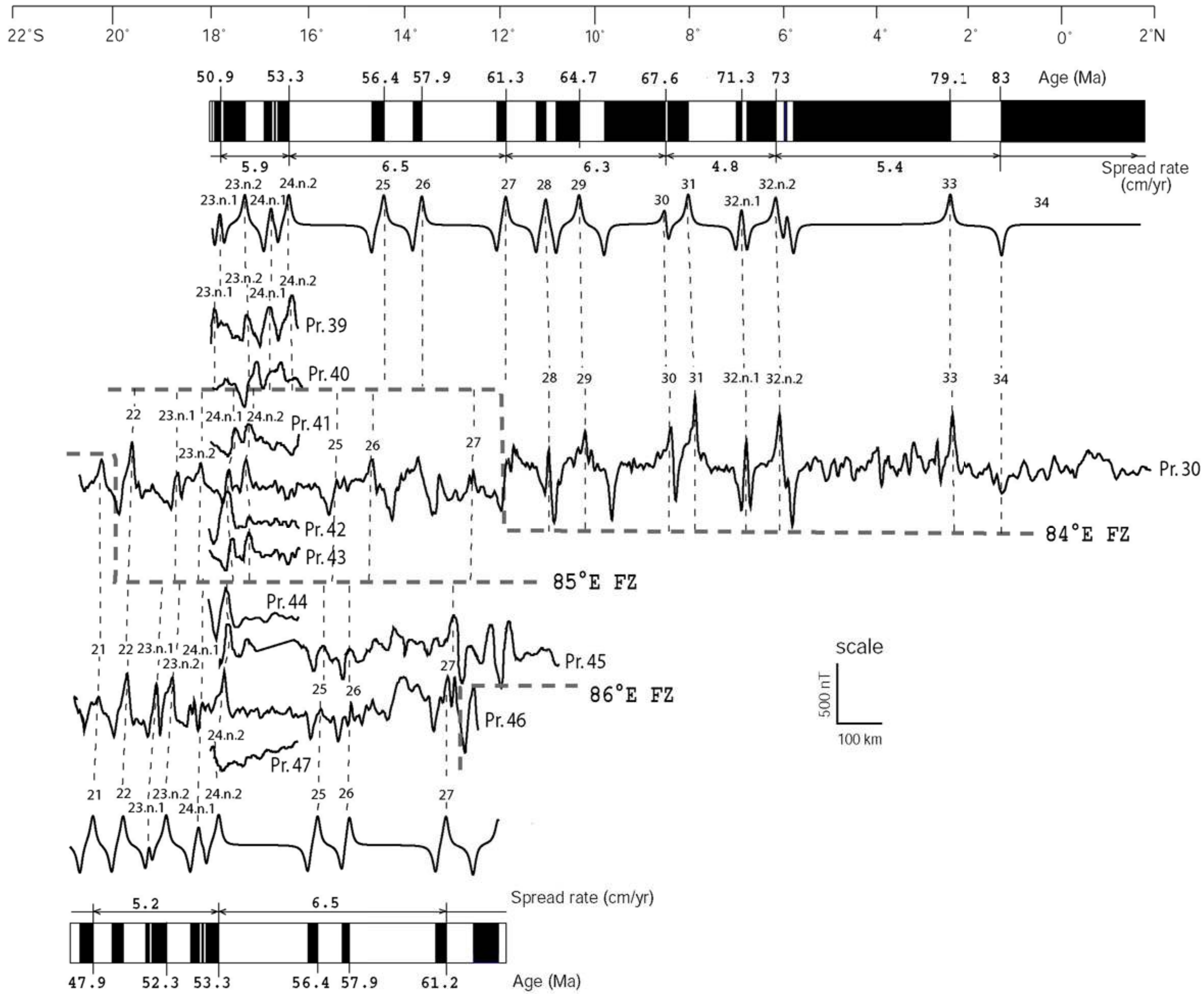

22°S
20°
18°
16°
14°
12°
10°
8°
6°
4°
2°
0°
2°N
50.9
53.3
56.4
57.9
61.3
64.7
67.6
71.3
73
79.1
83
Age (Ma)
5.9
6.5
6.3
4.8
5.4
Spread rate (cm/yr)
Pr. 39
Pr. 40
Pr. 41
Pr. 30
Pr. 42
Pr. 43
Pr. 44
Pr. 45
Pr. 46
Pr. 47
84°E FZ
85°E FZ
86°E FZ
scale
500 nT
100 km
5.2
6.5
Spread rate (cm/yr)
47.9
52.3
53.3
56.4
57.9
61.2
Age (Ma)

Figure 4a

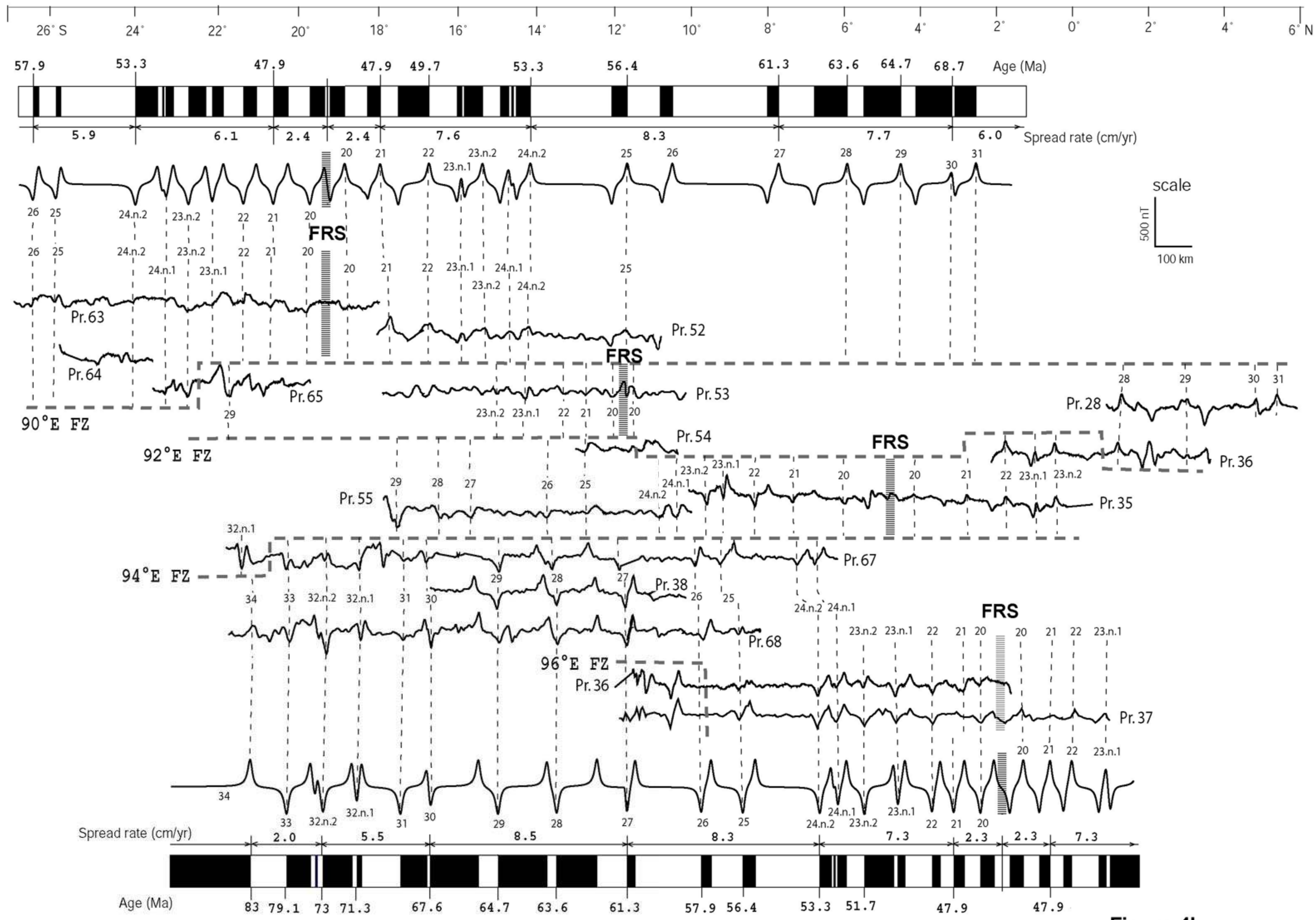

26° S
24°
22°
20°
18°
16°
14°
12°
10°
8°
6°
4°
2°
0°
2°
4°
6° N
Age (Ma)
Spread rate (cm/yr)
scale
500 nT
100 km
FRS
Pr. 63
Pr. 64
Pr. 65
Pr. 52
Pr. 53
Pr. 54
Pr. 55
Pr. 28
Pr. 36
Pr. 35
Pr. 67
Pr. 38
Pr. 68
Pr. 37
90°E FZ
92°E FZ
94°E FZ
96°E FZ

Figure 4b

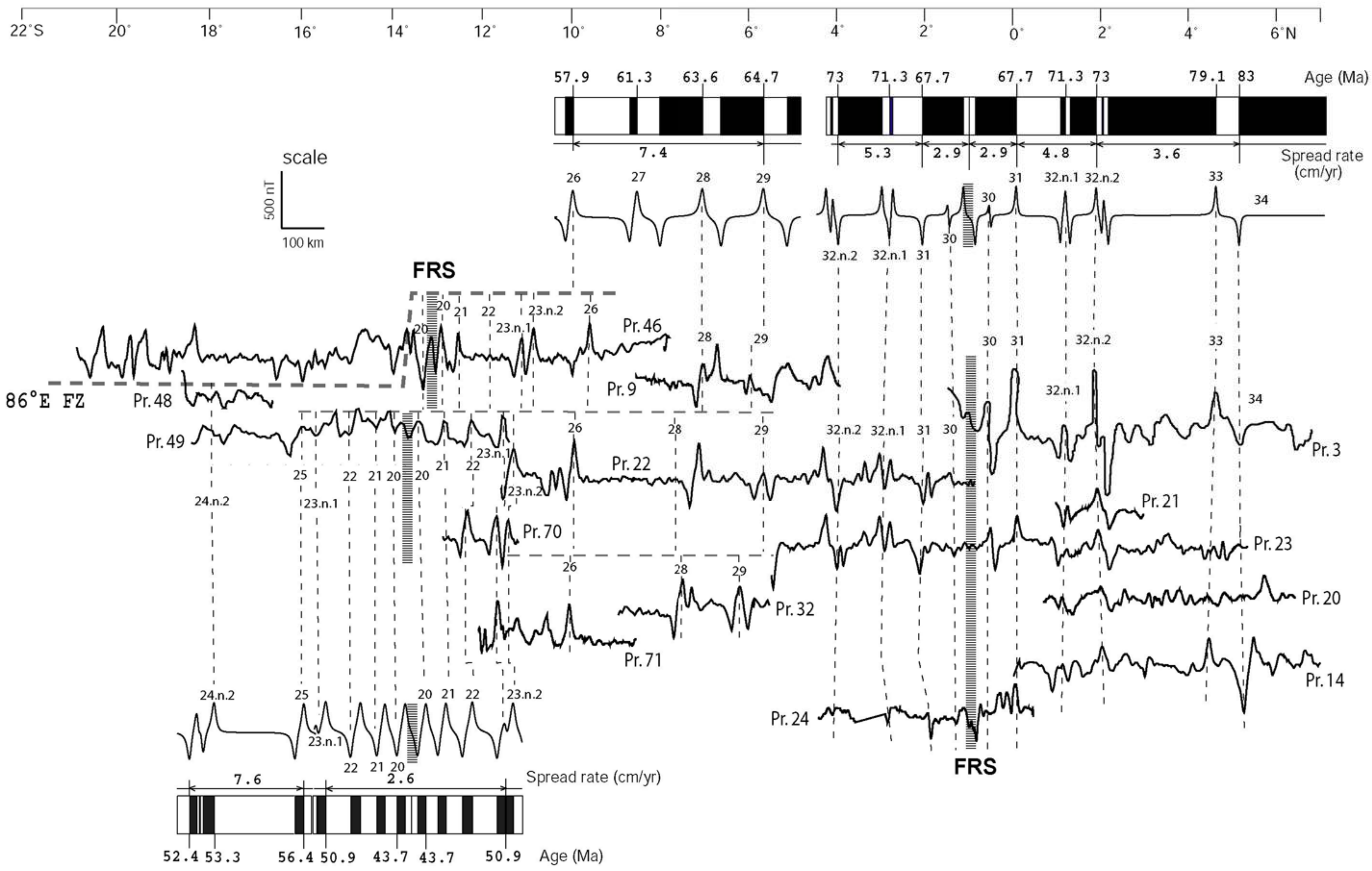
22°S 20° 18° 16° 14° 12° 10° 8° 6° 4° 2° 0° 2° 4° 6°N
Age (Ma)
57.9 61.3 63.6 64.7
73 71.3 67.7 67.7 71.3 73 79.1 83
Spread rate (cm/yr)
7.4
5.3 2.9 2.9 4.8 3.6
scale
500 nT
100 km
FRS
86°E FZ
Pr. 46
Pr. 48
Pr. 49
Pr. 9
Pr. 3
Pr. 22
Pr. 21
Pr. 70
Pr. 23
Pr. 32
Pr. 20
Pr. 71
Pr. 14
Pr. 24
FRS
Spread rate (cm/yr)
7.6
2.6
52.4 53.3 56.4 50.9 43.7 43.7 50.9
Age (Ma)

Figure 4c

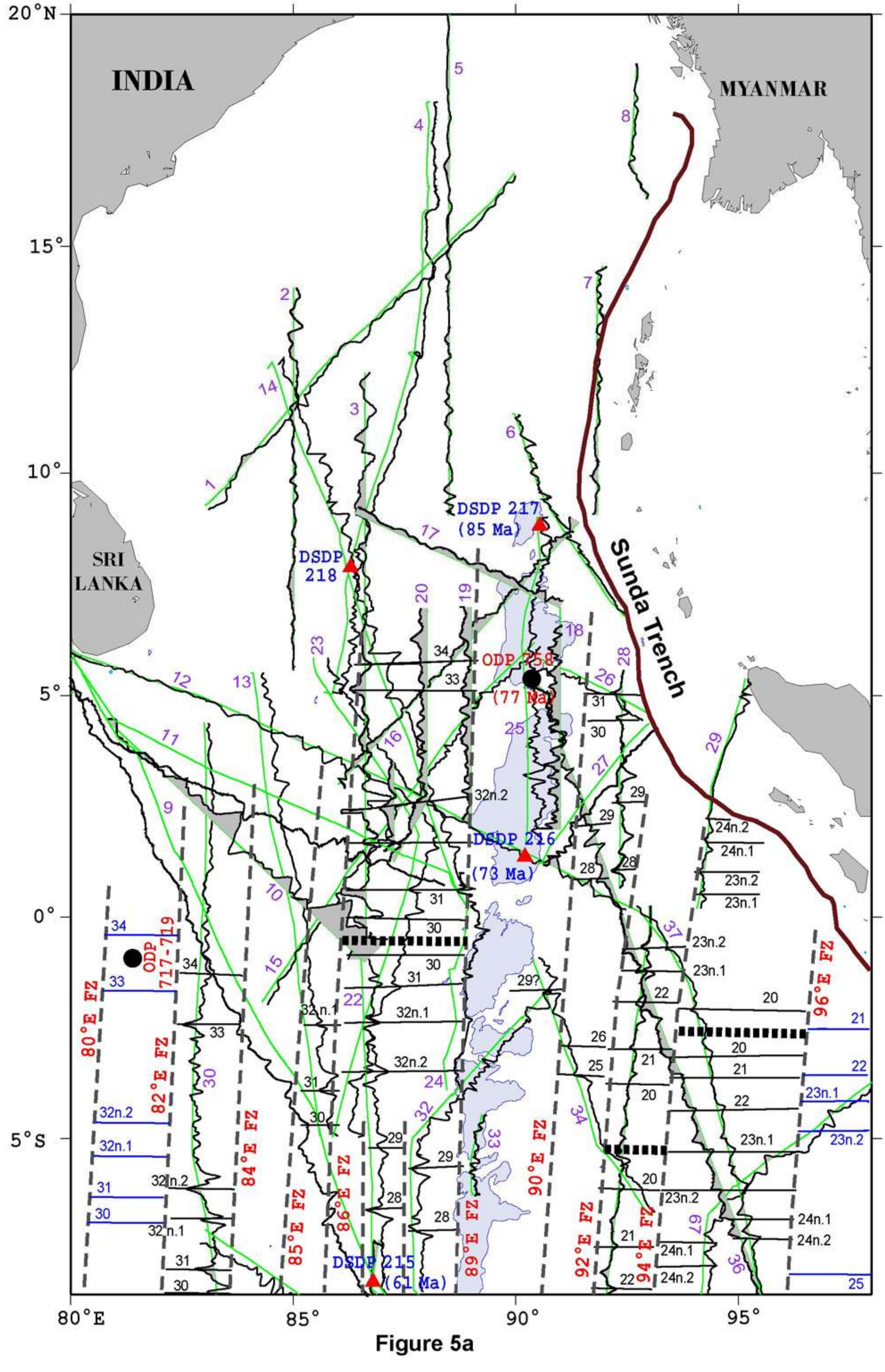
INDIA
MYANMAR
SRI LANKA
Sunda Trench
DSDP 217 (85 Ma)
DSDP 218
ODP 758 (77 Ma)
DSDP 216 (73 Ma)
DSDP 215 (61 Ma)
ODP 717-719
80°E FZ
82°E FZ
84°E FZ
85°E FZ
86°E FZ
89°E FZ
90°E FZ
92°E FZ
94°E FZ
96°E FZ
20°N
15°
10°
5°
0°
5°S
80°E
85°
90°
95°

Figure 5a

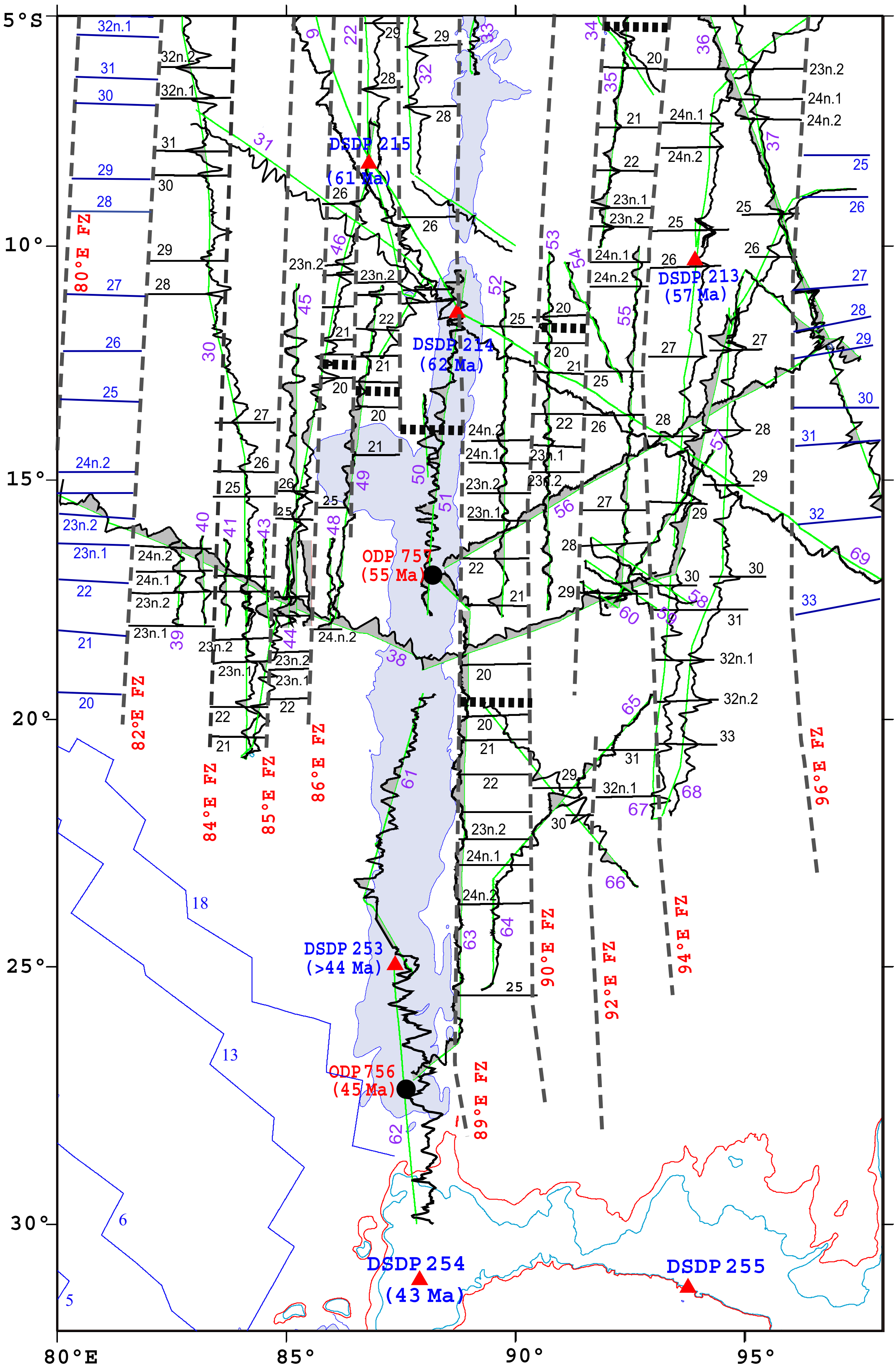
5°S
10°
15°
20°
25°
30°
80°E
85°
90°
95°
80°E FZ
82°E FZ
84°E FZ
85°E FZ
86°E FZ
89°E FZ
90°E FZ
92°E FZ
94°E FZ
96°E FZ
DSDP 215
(61 Ma)
DSDP 214
(62 Ma)
DSDP 213
(57 Ma)
ODP 757
(55 Ma)
DSDP 253
(>44 Ma)
ODP 756
(45 Ma)
DSDP 254
(43 Ma)
DSDP 255

Figure 5b

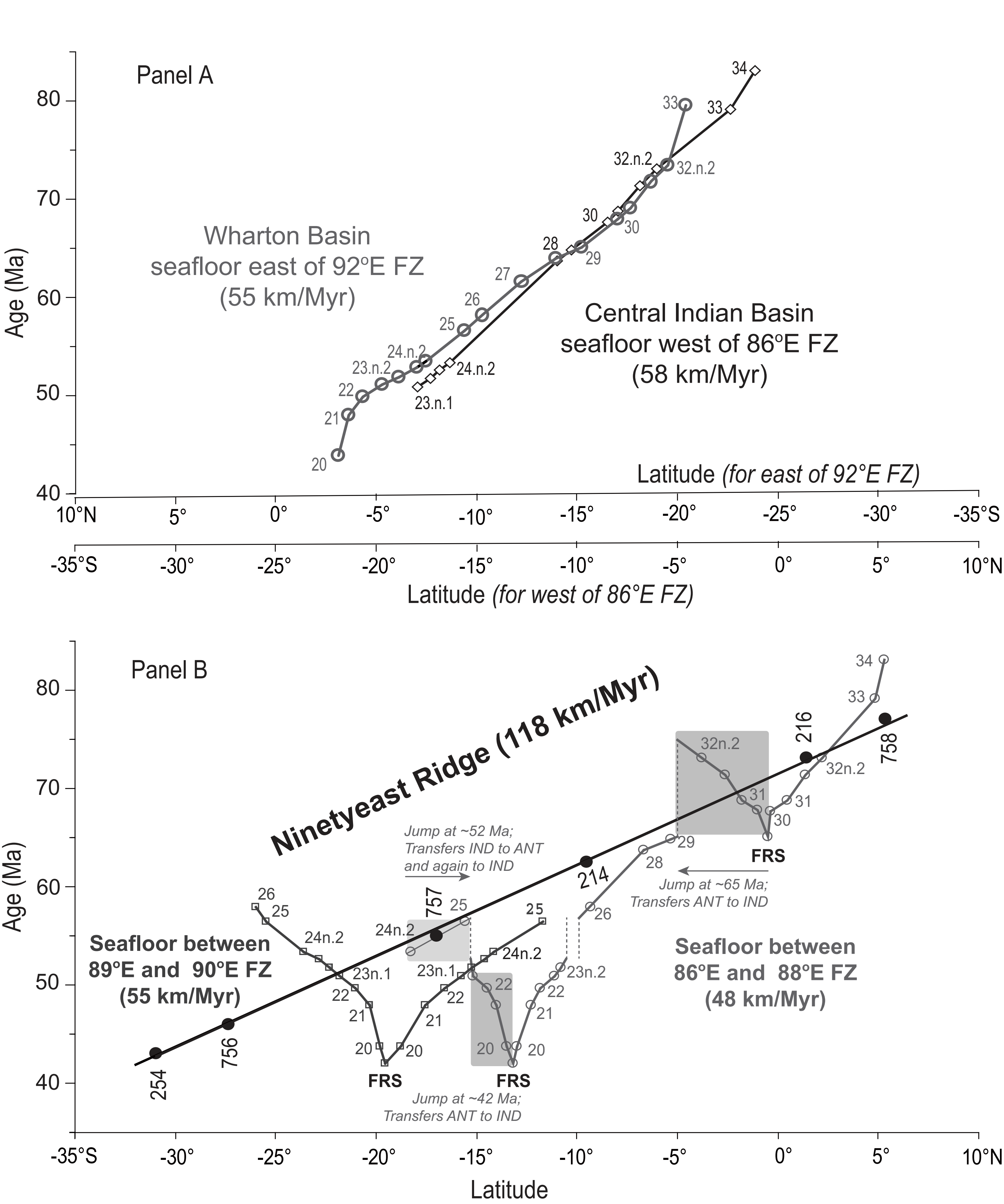
Panel A
Age (Ma)
Wharton Basin
seafloor east of 92°E FZ
(55 km/Myr)
Central Indian Basin
seafloor west of 86°E FZ
(58 km/Myr)
Latitude (for east of 92°E FZ)
Latitude (for west of 86°E FZ)
Panel B
Ninetyeast Ridge (118 km/Myr)
Seafloor between
89°E and 90°E FZ
(55 km/Myr)
Seafloor between
86°E and 88°E FZ
(48 km/Myr)
Jump at ~52 Ma;
Transfers IND to ANT
and again to IND
Jump at ~65 Ma;
Transfers ANT to IND
Jump at ~42 Ma;
Transfers ANT to IND
FRS
Latitude

Figure 6

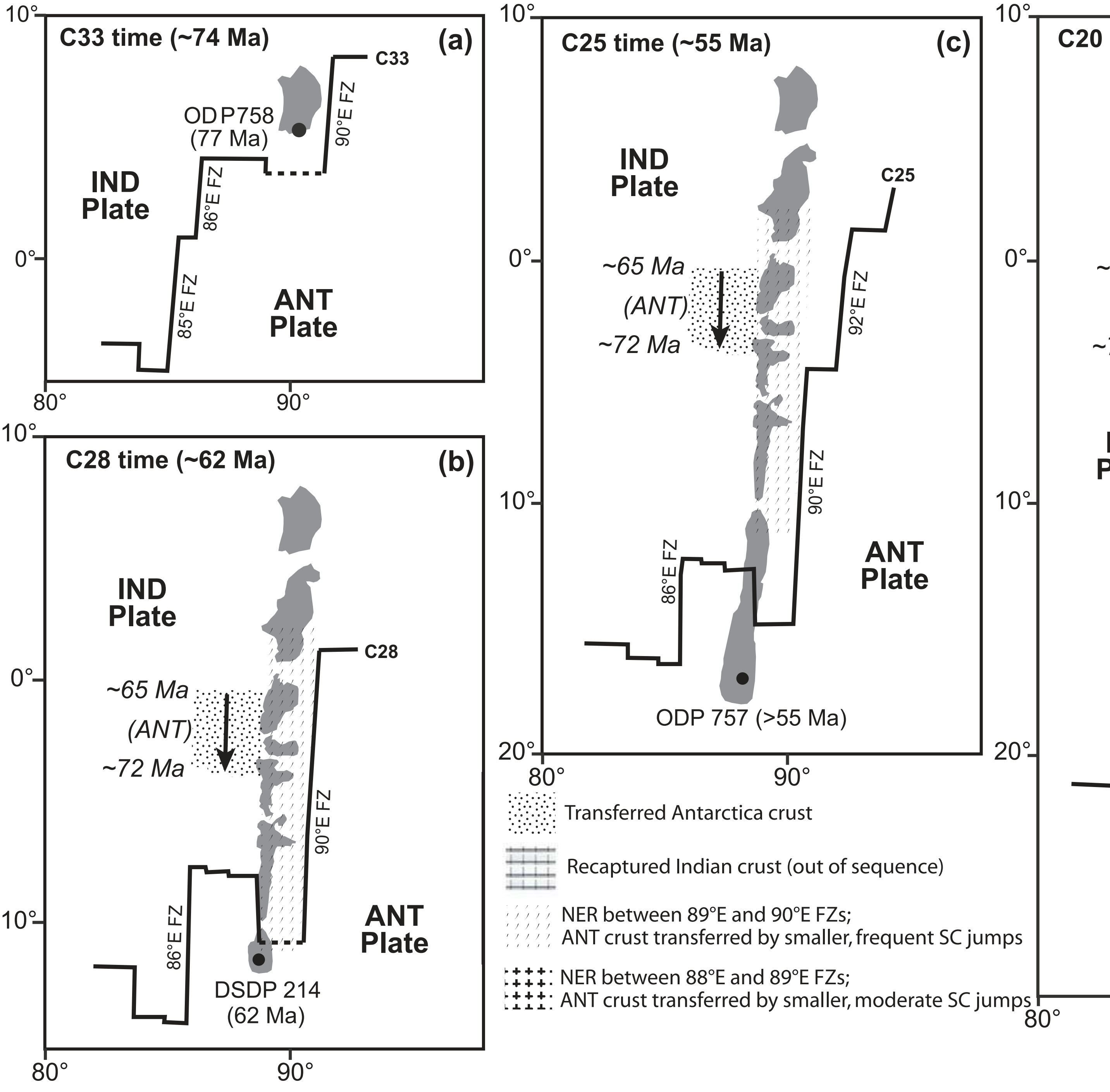
C33 time (~74 Ma)
(a)
C33
ODP758
(77 Ma)
90°E FZ
86°E FZ
85°E FZ
IND
Plate
ANT
Plate
10°
0°
80°
90°
C28 time (~62 Ma)
(b)
C28
IND
Plate
~65 Ma
(ANT)
~72 Ma
90°E FZ
86°E FZ
DSDP 214
(62 Ma)
ANT
Plate
C25 time (~55 Ma)
(c)
C25
IND
Plate
~65 Ma
(ANT)
~72 Ma
92°E FZ
90°E FZ
86°E FZ
ANT
Plate
ODP 757 (>55 Ma)
20°
C20
Transferred Antarctica crust
Recaptured Indian crust (out of sequence)
NER between 89°E and 90°E FZs;
ANT crust transferred by smaller, frequent SC jumps
NER between 88°E and 89°E FZs;
ANT crust transferred by smaller, moderate SC jumps

Figure 7

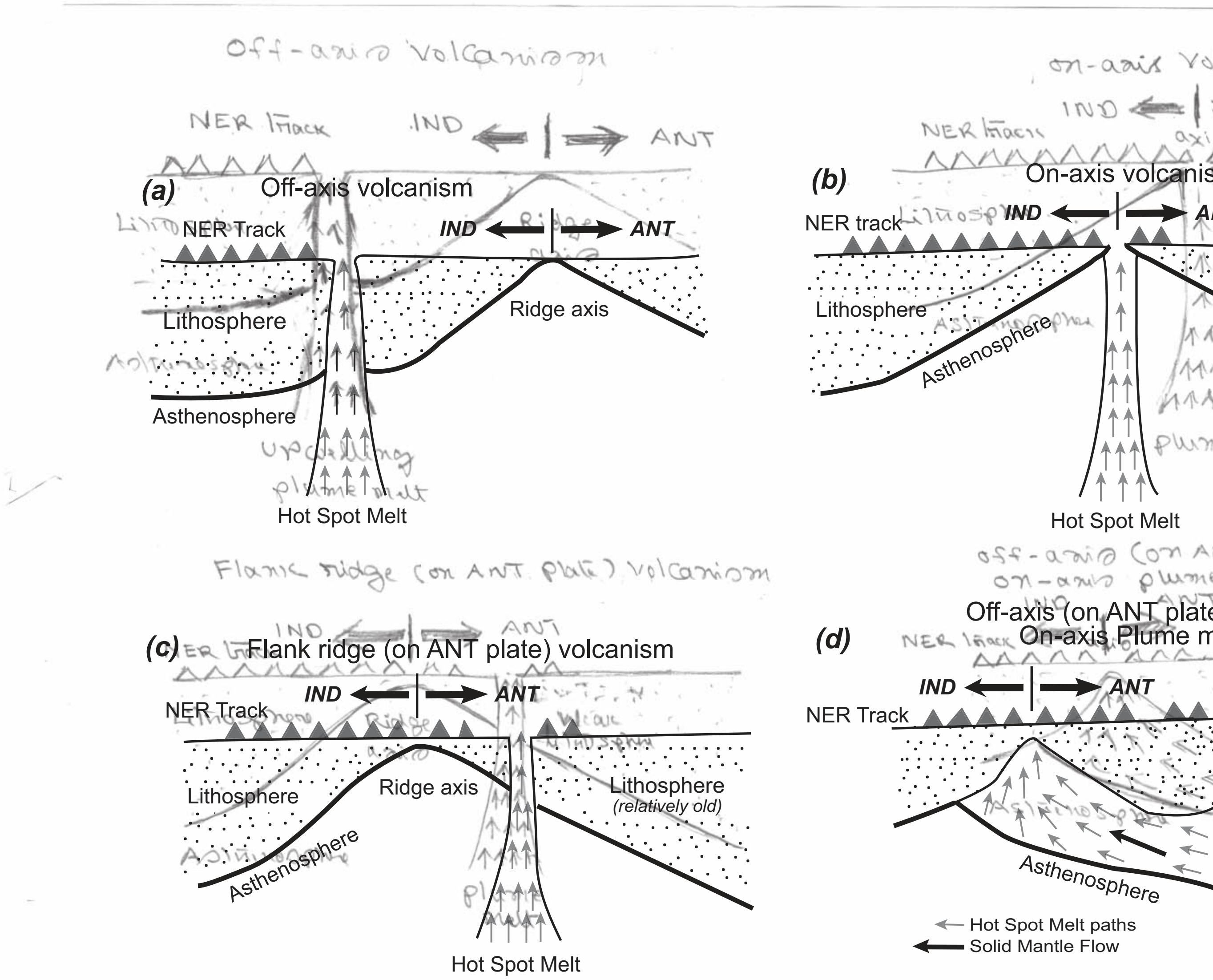
(a)
Off-axis volcanism
NER Track
IND
ANT
Lithosphere
Ridge axis
Asthenosphere
Hot Spot Melt
(b)
NER track
IND
Lithosphere
Asthenosphere
Hot Spot Melt
(c)
Flank ridge (on ANT plate) volcanism
NER Track
IND
ANT
Lithosphere
Ridge axis
Lithosphere
(relatively old)
Asthenosphere
Hot Spot Melt
(d)
NER Track
IND
ANT
Asthenosphere
Hot Spot Melt paths
Solid Mantle Flow

Figure 8

Table 1: Details of profiles ids and data bases used in the present study

Profile Number used in the present study	Original Profile id	Research vessel used for the data acquisition	Data Source
1	CIRC03AR	R/V Argo	NGDC
2	SK82- 14	ORV Sagar Kanya	NIO database
3	SK82-02	ORV Sagar Kanya	NIO database
4	ANTP11MV	R/V Melville	NGDC
5	SK100-10	ORV Sagar Kanya	NIO database
6	CIRC03AR	R/V Argo	NGDC
7	SK100-20	ORV Sagar Kanya	NIO database
8	CIRC03AR	R/V Argo	NGDC
9	WILKES815	USNS Wilkes	NGDC
10	SK82-01	ORV Sagar Kanya	NIO database
11	WILKES907	USNS Wilkes	NGDC
12	C0909	R/V Conrad	NGDC
13	C0909	R/V Conrad	NGDC
14	INMDO6MV	R/V Melville	NGDC
15	CIRC03AR	R/V Argo	NGDC
16	SK100-01c	ORV Sagar Kanya	NIO database
17	SK124-5	ORV Sagar Kanya	NIO database
18	SK124-6	ORV Sagar Kanya	NIO database
19	SK124-8	ORV Sagar Kanya	NIO database
20	SK124-10	ORV Sagar Kanya	NIO database
21	SK124-12	ORV Sagar Kanya	NIO database
22	DSDP22GC	R/V Glomar Challenger	NGDC
23	C1709	R/V Conrad	NGDC
24	WILKES907	USNS Wilkes	NGDC
25	CIRC03AR	R/V Argo	NGDC
26	RC1402	R/V Robert Conrad	NGDC
27	DSDP22GC	R/V Glomar Challenger	NGDC
28	8400121b	R/V Jean Charcot	NGDC
29	LUSI7BAR	R/V Argo	NGDC
30	CIRC05AR	R/V Argo	NGDC
31	RC1402	R/V Robert Conrad	NGDC
32	RC1402	R/V Robert Conrad	NGDC
33	KNOX06RR	R/V Roger Revelle	NGDC
34	INMDO6MV	R/V Melville	NGDC
35	8400121a	R/V Jean Charcot	NGDC
36	ODP121JR	Joides Resolution	NGDC
37	C0909	R/V Conrad	NGDC
38	MONS3AR	R/V Argo	NGDC

39	TIOG-7	R/V Issledovatl	ILTP database
40	TIOG-8	R/V Issledovatl	ILTP database
41	TIOG-9	R/V Issledovatl	ILTP database
42	TIOG-10	R/V Issledovatl	ILTP database
43	TIOG-11	R/V Issledovatl	ILTP database
44	TIOG-12	R/V Issledovatl	ILTP database
45	TIOG-13	R/V Issledovatl	ILTP database
46	CIRC05AR-B	R/V Argo	NGDC
47	TIOG-14	R/V Issledovatl	ILTP database
48	TIOG-15	R/V Issledovatl	ILTP database
49	TIOG-16	XVII Syezo Profsoyuzov	ILTP database
50	KNOX06RR	R/V Roger Revelle	NGDC
51	TIOG-17	XVII Syezo Profsoyuzov	ILTP database
52	TIOG-18	XVII Syezo Profsoyuzov	ILTP database
53	TIOG-19	XVII Syezo Profsoyuzov	ILTP database
54	TIOG-20	XVII Syezo Profsoyuzov	ILTP database
55	TIOG-21	XVII Syezo Profsoyuzov	ILTP database
56	ODP121JR	Joides Resolution	NGDC
57	TIOG-51	XVII Syezo Profsoyuzov	ILTP database
58	TIOG-60	XVII Syezo Profsoyuzov	ILTP database
59	TIOG-61	XVII Syezo Profsoyuzov	ILTP database
60	TIOG-62	XVII Syezo Profsoyuzov	ILTP database
61	KNOX06RR	R/V Roger Revelle	NGDC
62	DSDP26GC	R/V Glomar Challenger	NGDC
63	ODP121JR	Joides Resolution	NGDC
64	KNOX06RR	R/V Roger Revelle	NGDC
65	KNOX06RR	R/V Roger Revelle	NGDC
66	CIRC05AR	R/V Argo	NGDC
67	ANTP12MVa	R/V Melville	NGDC
68	ANTP12MVb	R/V Melville	NGDC
69	WILKES815	USNS Wilkes	NGDC
70	CIRC05AR-C	R/V Argo	NGDC
71	WILKES907	USNS Wilkes	NGDC